공학석사학위논문

Extraction of Flutter Derivatives Based on the Force Controlled Forced Vibration Test

하중제어 강제가진 실험을 통한
플러터 계수 추출

2015년 2월

서울대학교 대학원

건설환경공학부

차 승 헌

ABSTRACT

This study presents a new excitation technique for the identification of flutter derivatives. When motion of a bridge perturbs the flow field, perturbed flow field induces a dynamic forces on a bridge. And the dynamic forces changes the motion of a bridge which perturbs the flow field again. This recursive nonlinear-interaction between movement of the section model and the flow field can be fully considered when prescribed excitation force is applied to the bridge section model without restraining the motion. Force controlled forced vibration test is conducted to check the effect of nonlinear interaction by comparing its flutter derivatives to those of displacement controlled forced vibration test. Sinusoidal force is enforced with four fan-shaped mass rotating on each corner of the model which is freely suspended on elastic springs.

An Equation Error Estimation method (EEE) is employed to evaluate flutter derivatives, which is the minimization problem of the equation error of the equation of motion. However, when L_2-Norm EEE is adopted, squared error lasts through minimization and leads to biased result. To examine the adequacy of L_2-Norm EEE to this problem, L_1-Norm EEE is composed utilizing a simplex algorithm. Since the amount of bias is not noticeable, L_2-Norm EEE is used throughout this paper for its fast computing speed.

The validity of the force controlled forced vibration test is demonstrated for two

examples, one is B/D=5 rectangular section and the other is Jido bridge section model. It can be said that the effect of nonlinear interaction can be ignored for bridge section for its small amount of influence on the flutter derivatives and time-domain aeroelastic analysis result.

KEY WORDS:

Flutter derivative; Equation error estimation; FDM-FIR filter; Forced vibration test; Aeroelastic analysis; Simplex algorithm

Student Number: 2013-20942

Table of Contents

List of Figures

List of Tables

1. Introduction

Long span bridge has been increased considerably in recent decades for its pragmatic and artistic feature. But as its span length expanded, several collapses were witnessed and importance of wind-resistant engineering has arisen. Low damping ratio and high flexibility make long span bridge sensitive to wind load and thus examinations, such as flutter analysis and buffeting analysis have been necessarily performed. It is highly challenging to develop analytic model for implementing CFD (Computational Fluid Dynamics), since bridge section model is bluff body and thus the interaction between bridge motion and wind load is extremely complex. Therefore experimental method is yet the most reliable tool.

Aerodynamic force induced by wind acts on the bridge and the motion of a bridge changes. The motion of a bridge perturbs the flow field and changed flow field recursively affect on the motion of a bridge as the form of aerodynamic force. This load effect related to the displacement and the velocity of a bridge is called aerodynamic stiffness and aerodynamic damping respectively. The interaction is intricate and proper experiment need to be carried out to consider its nonlinear effect. Generally, the assumption that the aerodynamic force to be linear combination of displacement and velocity of the bridge section made by Scanlan and Tomko (1971) is used. 2-DOF model with vertical and torsional movement is widely adopted and coefficients which act as aerodynamic damping and stiffness for displacement and velocity are called the

flutter derivatives.

The flutter derivatives can be evaluated through various experimental method which includes free vibration test and forced vibration test. Scanlan and Tomko (1971) proposed the flutter derivatives to model self-excited force with two basic assumptions that the motion of a section model is sinusoidal with small amplitude and in steady-state motion. Various experimental techniques were developed to evaluate flutter derivatives. Free vibration test which is simple and easy to execute, is widely adopted technique. With section model supported by springs without constraining its movement, the interaction can be fully considered and natural frequency and amplitude of motion can be controlled by moving springs and changing its stiffness. Initial condition is given for each DOF and motion history with decaying amplitude is observed to extract flutter derivatives. However, despite its simplicity of execution, extracting procedure is relatively hard. Since the flutter derivatives indicates system property such as damping and stiffness, it becomes an inverse analysis problem. For past years, different evaluation methods were made for free vibration test [Bartoli 2009, Chen 2004, Chowdhury 2003, Gu 2000, Iwamoto 1995, Li 2003, Matsumoto 1993, Sarkar 1992 and Sarkar 1994]. But free vibration test cannot maintain steady-state motion at high wind speed due to strong system damping.

The forced vibration test [Diana 2004, Falco 1992, Kim 2007 and Matsumoto 1993] is reliable method and in general use. The section model is rigidly connected to the driving equipment and prescribed displacement is imposed. Since it demands complex instruments, small number of laboratories are capable of this method. Enforced

2

movement keeps the section model in steady-state motion which satisfies the assumption and single frequency motion can be achieved at high wind speed, which was unable to attain through free vibration test. However, because it restraint the motion of section model, the interaction cannot be considered.

A new technique to extract flutter derivatives can obtain steady-state motion while the interaction is fully considered and requires relatively simple and movable driving equipment. Suspending a section model on elastic springs, rotating pendulums create heaving and pitching moment. Different from the displacement controlled forced vibration test, information of velocity and acceleration is needed as well. The FDM-FIR filter is thus utilized to generate such information from measured displacement. An equation error estimation (EEE) method which is proposed by Hong (2012) is employed for identification algorithm. Minimization of EEE can be done using different norms, however, measured error might remain as a form of bias when L_2-Norm is used. Using mechanical properties of a rectangular section on research of Park et al. (2014), time history data is constructed to verify norms for EEE.

The effect of nonlinear interaction is identified through two examples: a rectangular section with a width to depth (B/D) ratio of 5, Jido bridge section model. A new extraction technique yields similar flutter derivatives compared to that of the displacement controlled forced vibration method. And time-domain aeroelastic analysis and frequency-domain aeroelastic analysis also yields very similar result. The nonlinear effect of interaction can be neglected for general bridge section.

3

2. New Identification Method for Flutter Derivatives

2.1. Brief Overview for Existing Method

Among conventional methods, the displacement controlled forced vibration method is general method for extraction of flutter derivatives owing to its steady-state motion which complies with the assumption well. However its lack of interaction between the motion of a bridge and aerodynamic force might reduce the accuracy of flutter derivatives.
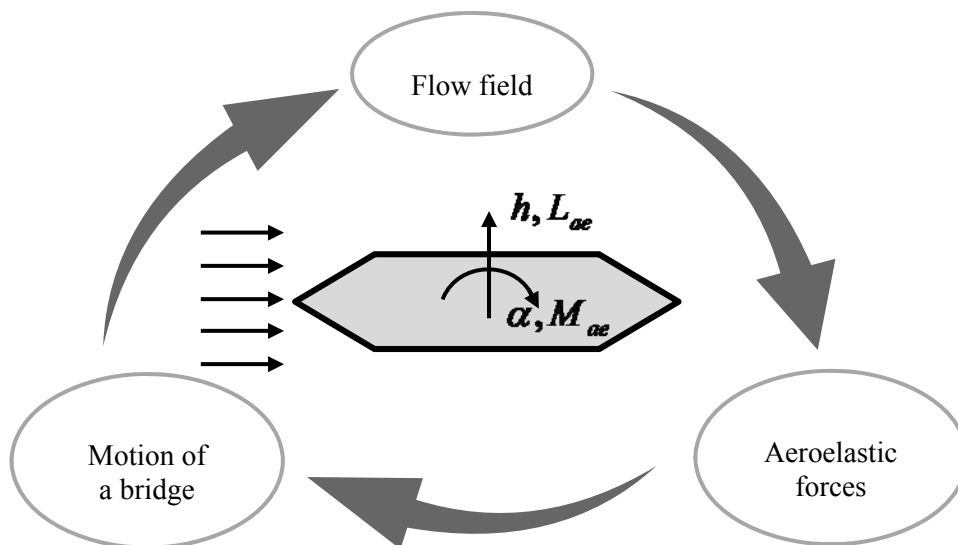
Fig. 2.1. Aeroelastic problem

Fig. 2.1. shows the interaction of aeroelastic problem of the bridge deck with the

wind flow. Restraining the motion of a bridge limits lower arrow, which stands for the effect of aerolastic forces on the motion of a bridge.

The equation of motion for forced vibration test includes external forcing term.

$$\mathbf{M}\ddot{\mathbf{u}}(t) + \mathbf{C}\dot{\mathbf{u}}(t) + \mathbf{K}\mathbf{u}(t) = \mathbf{F}_{ae}(t) + \mathbf{F}_{ex}(t) \tag{2.1}$$

where $\mathbf{M}$, $\mathbf{C}$, $\mathbf{K}$, $\mathbf{F}_{ae}$ and $\mathbf{F}_{ex}$ represent the mass, damping, stiffness matrix of a structure and an aeroelastic force and an external force, respectively, while $\mathbf{u} = (h \quad \alpha)^T$ denote the displacement of the structure.

The aeroelastic force induced by the motion of a bridge is assumed as a linear function to the displacement and velocity of the bridge section [Iwamoto 1995 and Scanlan 1971]

$$\begin{aligned}
\mathbf{F}_{ae}(t) &= \begin{pmatrix} L_{ae}(t) \\ M_{ae}(t) \end{pmatrix} \approx \mathbf{C}_{ae}(\omega)\dot{\mathbf{u}}(t) + \mathbf{K}_{ae}(\omega)\mathbf{u}(t) \\
&= \begin{bmatrix} H_1(\omega) & H_2(\omega) \\ A_1(\omega) & A_2(\omega) \end{bmatrix} \begin{pmatrix} \dot{h}(t) \\ \dot{\alpha}(t) \end{pmatrix} + \begin{bmatrix} H_4(\omega) & H_3(\omega) \\ A_4(\omega) & A_3(\omega) \end{bmatrix} \begin{pmatrix} h(t) \\ \alpha(t) \end{pmatrix}
\end{aligned} \tag{2.2}$$

where L_{ae} and M_{ae} are the aeroelastic lift force and momet, respectively, while ω is the circular frequency of the oscillation, and H_i and A_i (i = 1, 2, 3, 4) are the flutter derivatives of oscillating section. Since the steady-state response of section model is in single frequency, the flutter derivatives are defined in certain frequency.

Substitution of Eq. (2.2) to Eq. (2.1) yields following equation.

$$\mathbf{M}\ddot{\mathbf{u}}(t) + \mathbf{C}_{eff}\dot{\mathbf{u}}(t) + \mathbf{K}_{eff}\mathbf{u}(t) = \mathbf{F}_{ex}(t) \qquad (2.3)$$

where $\mathbf{C}_{eff}$ and $\mathbf{K}_{eff}$ are effective damping and stiffness matrices of system as:

$$\mathbf{C}_{eff} = \mathbf{C} - \mathbf{C}_{ae}, \quad \mathbf{K}_{eff} = \mathbf{K} - \mathbf{K}_{ae} \qquad (2.4)$$

The prescribed sinusoidal displacement is imposed on the section model. One electrical motor rotates and rigid arm conveys its movement to the model into vertical and torsional motion. Imposing displacement is as follows

$$\mathbf{u}(t) = \begin{pmatrix} h_0 \\ \alpha_0 \end{pmatrix} \sin(\omega_{ex}t) \qquad (2.5)$$

where ω_{ex} is the exciting frequency of the prescribed displacement.

The reaction force in Eq. (2.3) is measured, and the steady-state response after the transient part damped out is:

$$\mathbf{F}_{ex}(t) = \begin{pmatrix} \overline{L}_s \\ \overline{M}_s \end{pmatrix} \sin(\omega_{ex}t) + \begin{pmatrix} \overline{L}_c \\ \overline{M}_c \end{pmatrix} \cos(\omega_{ex}t) \qquad (2.6)$$

where $\overline{L}_s$, $\overline{L}_c$, $\overline{M}_s$ and $\overline{M}_c$ are the measured amplitudes of sinusoidal response, the reaction force of Eq. (2.3)

6

Substitution of Eq. (2.6) and Eq. (2.5) into Eq. (2.3) yields following equations

$$\left(\frac{\overline{L}_s}{\overline{M}_s} \right) = \left[-\omega_{ex}^2 \mathbf{M} + \mathbf{K}_{eff} \right] \begin{Bmatrix} h_0 \\ \alpha_0 \end{Bmatrix}, \quad \left(\frac{\overline{L}_c}{\overline{M}_c} \right) = \omega_{ex} \mathbf{C}_{eff} \begin{Bmatrix} h_0 \\ \alpha_0 \end{Bmatrix} \tag{2.7}$$

Above equations are linear to unknown variables, $\mathbf{C}_{eff}$ and $\mathbf{K}_{eff}$. Two different displacement controlled test ought to be carried out since one test yields 4 equations and unknown variables are 8 total. Once amplitudes for the reaction force and displacement, the flutter derivatives are easily derived through analytic process.

2.2 Force Controlled Forced Vibration Test

The force controlled forced vibration test is similar to the displacement controlled forced vibration test. In analytic aspect, the input and output is switched as the force is imposed and the displacement is measured. This might leads to the similar result but the biggest difference between two test methods is the consideration of interaction. In the force controlled test, the motion of a section model is not constrained and suspended by elastic springs the same as in the free vibration test, without restriction. As Fig. 2.1. describes, when the motion of a section model perturbs the flow field and the aerodynamic forces change, the motion of a section model should be changed due to the change in the aerodynamic forces. This nonlinearity can be fully considered in the force controlled test yet how critical this effect be is not known. The nonlinear effect of interaction is need to be checked as the displacement controlled test has its limit that testing process is linearly constrained and aerodynamic force also is also assumed to be linear. Thus testing mechanism should reflect real bridge motion which is nonlinear.

Fig. 2.2. Exciting mechanism of the force controlled forced vibration test

8

Shown in Fig. 2.2. above, total 4 motors attached to the metal guide rotates pendulum to generate centrifugal force. Each coupled forces combined and remaining force is applied to shake the section model in 2-DOF motion. In this way, two assumptions made by Scanlan (1971) are both satisfied: sinusoidal and steady-state motion.

The displacement of the section model is steady-state response of Eq. (2.3) induced by exciting force as follows

$$\mathbf{F}_{ex}(t) = \begin{pmatrix} L_{ex}(t) \\ M_{ex}(t) \end{pmatrix} = \begin{pmatrix} L_0 \\ M_0 \end{pmatrix} \sin(\omega_{ex} t) \tag{2.8}$$

After the transient response damped out, the displacement is:

$$\mathbf{u}(t) = \begin{pmatrix} h_s \\ \alpha_s \end{pmatrix} \sin(\omega_{ex} t) + \begin{pmatrix} h_c \\ \alpha_c \end{pmatrix} \cos(\omega_{ex} t) \tag{2.9}$$

Substitution of Eq. (2.8) and Eq. (2.9) to Eq. (2. 3) yields following equations

$$\begin{pmatrix} h_c \\ \alpha_c \end{pmatrix} = -\left[\left(-\omega_{ex}^2 \mathbf{M} + \mathbf{K}_{eff} \right) \left(\omega_{ex}^{-1} \mathbf{C}_{eff}^{-1} \right) \left(-\omega_{ex}^2 \mathbf{M} + \mathbf{K}_{eff} \right) + \left(\omega_{ex} \mathbf{C}_{eff} \right) \right]^{-1} \begin{pmatrix} L_0 \\ M_0 \end{pmatrix}$$

$$\begin{pmatrix} h_s \\ \alpha_s \end{pmatrix} = \left[\left(-\omega_{ex}^2 \mathbf{M} + \mathbf{K}_{eff} \right) + \omega_{ex} \mathbf{C}_{eff} \left(-\omega_{ex}^2 \mathbf{M} + \mathbf{K}_{eff} \right)^{-1} \omega_{ex} \mathbf{C}_{eff} \right]^{-1} \begin{pmatrix} L_0 \\ M_0 \end{pmatrix} \tag{2.10}$$

The same as the displacement controlled test, two separated tests must be con-

ducted due to the lack of information. However, even sufficient information is gathered, above equation is nonlinear to the unknown parameters, $\mathbf{C}_{eff}$ and $\mathbf{K}_{eff}$. Output error estimator (OEE) is difficult to be implemented since the sensitivity analysis for the equation is severely complex, thus analytic solution is hard to be derived, either.

Equation error estimator (EEE) proposed by Hong (2012) offers efficient way to evaluate the flutter derivatives from the force controlled test.

3. Filter and System Identification Method

3.1. FDM-FIR filter

As displacement is measured discretely by a time interval of Δt, generating acceleration should be employed in discretized fashion. The finite impulse response (FIR) filter is a digital filter that defines the relationship between the input values and the output values. In this section, a new approach to generate acceleration and velocity is presented as a boundary value problem. For given time interval, displacement at a fixed material point is fully measured by displacement meter. By definition, the minimization problem for generating acceleration is:

$$\text{Min}\Pi = \frac{1}{2}\int_T \left[\bar{u}(t) - \int_0^t \left(\int_0^t a(t)dt + \bar{v}(0) \right)dt + \bar{u}(0) \right]^2 dt \tag{3.1}$$

where $\bar{u}(t)$, $a(t)$ and $\bar{v}(0)$ are measured displacement, acceleration and measured initial velocity, respectively. This minimization problem is ill-posed and impossible to yield a unique acceleration as proper boundary condition is not known. The regularization technique that applies additional information, *a priori*, can estimate solution. The generated acceleration should stay around 0, the static value. Applying this regularization, Eq. (3.11) becomes:

11

$$\text{Min}\Pi = \frac{1}{2}\int_T \left[\bar{u}(t) - \int_0^t\left(\int_0^t a(t)dt + \bar{v}(0)\right)dt + \bar{u}(0)\right]^2 dt + \frac{\lambda}{2}\int_T a(t)^2 dt \qquad (3.2)$$

where λ is a regularization factor. By definition that acceleration is a second derivative of displacement about time, this equation becomes:

$$\text{Min}\Pi = \frac{1}{2}\int_T \left(\bar{u}(t) - u(t)\right)^2 dt + \frac{\lambda}{2}\int_T \left(\frac{d^2u(t)}{dt^2}\right)^2 dt \qquad (3.3)$$

In variational statement, above equation yields following governing equations.

$$u(t) - \bar{u}(t) + \lambda\frac{d^4u(t)}{dt^4} = 0, \quad \frac{d^2u(t)}{dt^2} = a(t) \qquad (3.4)$$

The transfer function of the governing equation Eq. (3.14) is derived by employing the Fourier transform.

$$F(u) = \frac{1}{1+\lambda\omega^4}F(\bar{u}), \quad F(a) = -\omega^2 F(u) \rightarrow F(a) = -\frac{\omega^2}{1+\lambda\omega^4}F(\bar{u}) \qquad (3.5)$$

$$H_{TF}(\omega) = -\frac{\omega^2}{1+\lambda\omega^4} = -\frac{(2\pi f)^2}{1+\lambda(2\pi f)^4} \qquad (3.6)$$

$$H_E(\omega) = -\omega^2 = -(2\pi f)^2 \qquad (3.7)$$

where H_{TF}, H_E and f denotes the transfer function, the exact transfer function and the frequency, respectively.

The accuracy of the generated acceleration is specified with the accuracy function, which is the ratio of the transfer function H_{TF} to the exact transfer function H_E. The accuracy function of the transfer function used in the acceleration generation, $H_{TF}^{acc}(\omega)$ is defined as follows.

$$H_{TF}^{acc}(\omega) = \frac{1}{1+\lambda\omega^4} = \frac{1}{1+\lambda(2\pi f)^4} \qquad (3.8)$$

It is convenient to normalize the transfer function and the accuracy function by the target frequency to make the frequency dimensionless. Normalized transfer function and accuracy functions are as follows

$$\widetilde{H}_{TF}(\widetilde{f}) = -\frac{H_{TF}(\omega)}{(2\pi f_T)^2} = \frac{\widetilde{f}^2}{1+\lambda(2\pi f)^4} \qquad (3.9)$$

$$\widetilde{H}_E(\widetilde{f}) = -\frac{H_E(\omega)}{(2\pi f_T)^2} = \frac{-(2\pi f)^2}{-(2\pi f_T)^2} = \widetilde{f}^2 \qquad (3.10)$$

$$\widetilde{H}_{TF}^{acc}(\widetilde{f}) = \frac{\widetilde{H}_{TF}(\widetilde{f})}{\widetilde{H}_E(\widetilde{f})} = \frac{1}{1+\lambda(2\pi f)^4} \qquad (3.11)$$

where $\widetilde{H}_{TF}$, $\widetilde{H}_E$, $\widetilde{H}_{TF}^{acc}$, f_T and $\widetilde{f} = f/f_T$ are the normalized transfer function, the normalized exact transfer function, the normalized accuracy function, the target frequency and the dimensionless frequency normalized to the target frequency, respectively.

The accuracy at the target frequency is attained by setting $\widetilde{f} = 1$ in Eq. (3.11).

$$\alpha_T = \frac{1}{1 + \lambda(2\pi f_T)^4} \tag{3.12}$$

where α_T is the target accuracy. The target accuracy may be chosen arbitrarily, in interval of $0 < \alpha_T \leq 1$ according to an engineering sense. The components related to the target frequency will be generated about the target accuracy, thus it means the desired accuracy. Once the target accuracy is selected, the regularization factor is determined as following.

$$\lambda = \frac{1}{(2\pi f_T)^4}\left(\frac{1}{\alpha_T} - 1\right) \ for \ \ 0 < \alpha_T \leq 1 \tag{3.13}$$

Substitution of Eq. (3.13) into Eq. (3.9) and Eq. (3.11) leads to the following expressions, respectively.

$$\widetilde{H}_{TF}(\widetilde{f}) = \frac{\widetilde{f}^2}{1 + (1/\alpha_T - 1)\widetilde{f}^4} \tag{3.14}$$

$$\widetilde{H}_{TF}^{acc}(\widetilde{f}) = \frac{1}{1 + (1/\alpha_T - 1)\widetilde{f}^4} \tag{3.15}$$

The transfer functions and the accuracy functions for different target accuracy are drawn in Fig. 3.1. and Fig 3.2., respectively. Compared with the exact function, the transfer function decreases fast as the exact function increases rapidly. For frequency
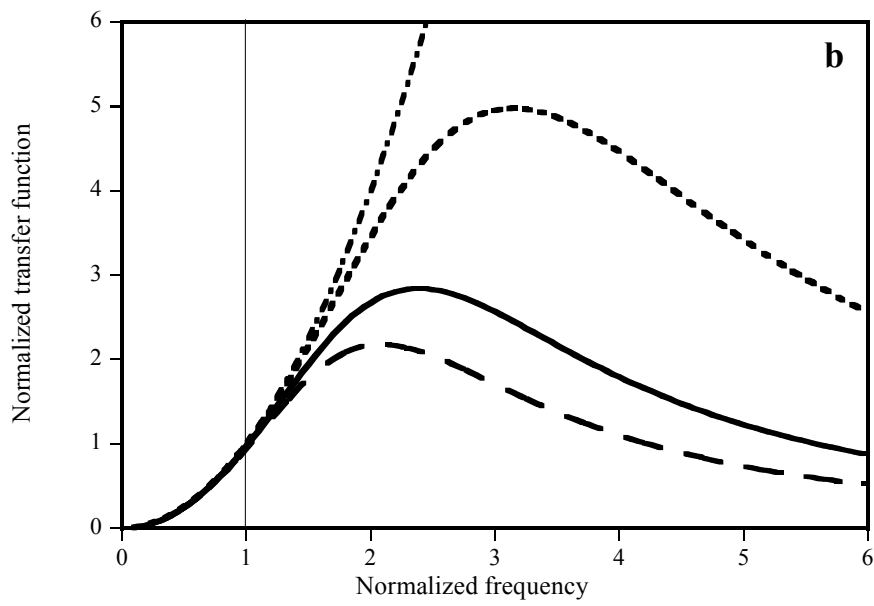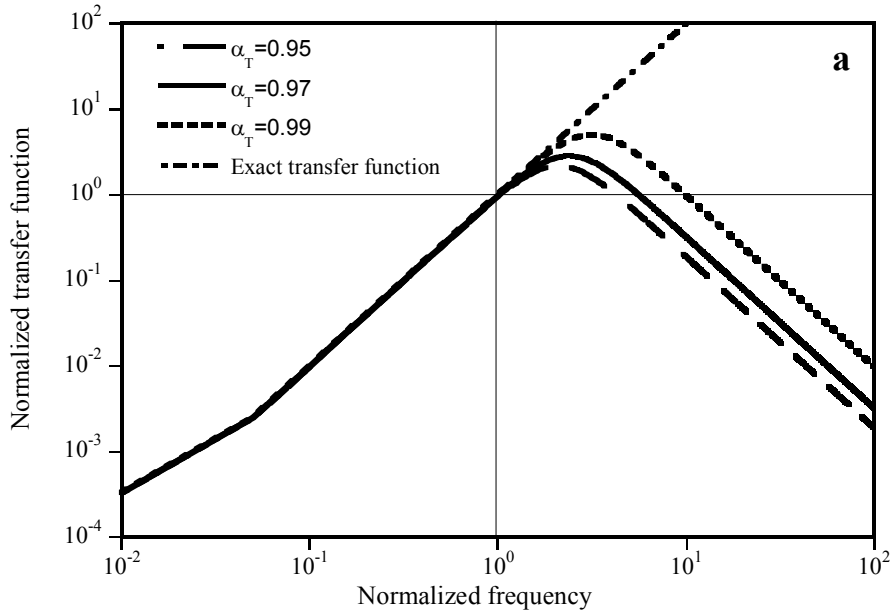
Fig. 3.1. Transfer functions for different target accuracy:

(a) Log-log scale. (b) Detail in a linear scale

15
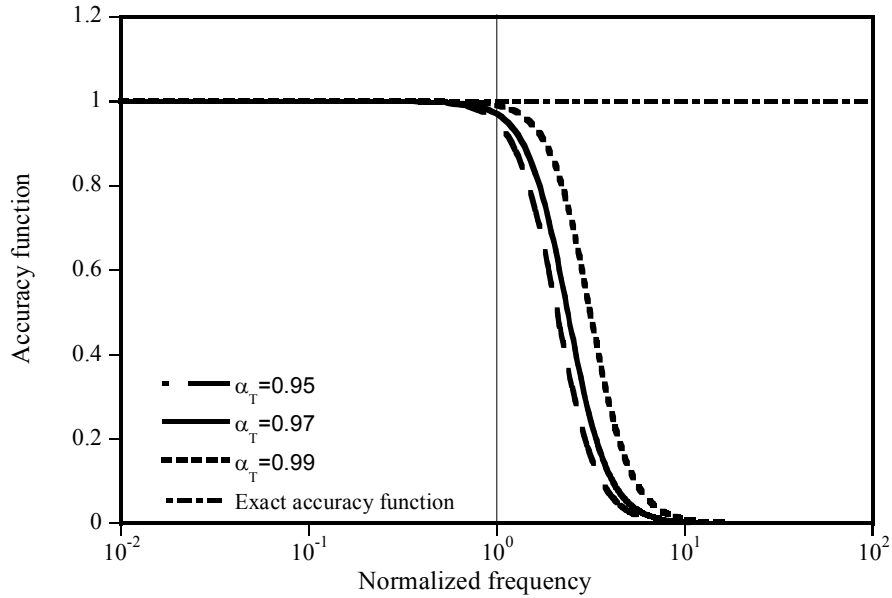
Fig. 3.2. Accuracy functions for different target accuracy

domain below the target frequency, both functions are almost identical. It shows this filter suppresses any noise which is in higher frequency range than the target frequency. Lower target accuracy yields stronger noise-suppression of the transfer function. In case high level noise is expected in measured displacement, lower target accuracy will be desirable for generating acceleration to apply strong noise suppression. The target accuracy of 0.97 is selected for filters in this paper.

 The FDM-FIR filter uses finite difference method to generate acceleration from the measured displacement and is formulated only in the time domain. Fig 3.3. demonstrates the arrangement for the FDM-FIR filter. A moving time window which contains $2k+1$ points of displacements in it, expresses the acceleration at the center of the

16
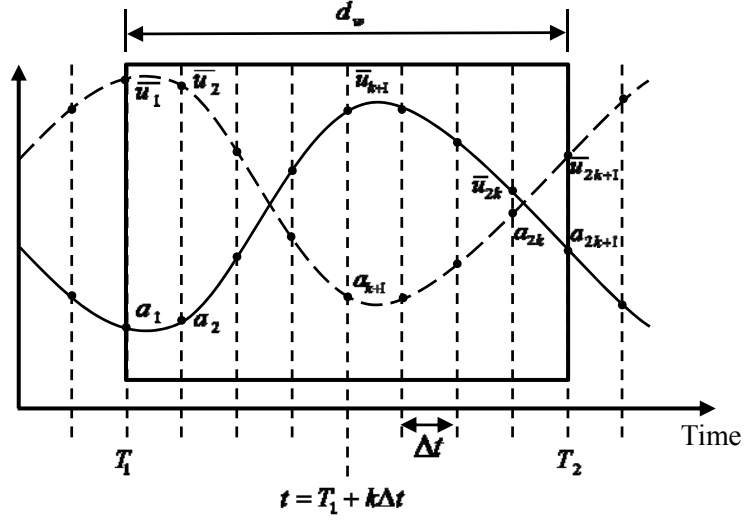
Fig. 3.3. A time window and measured displacements for FDM-FIR filter

time window, a_{k+1}, as a linear combination of measured displacements in a time window. Once the time window size, which is referred to as the filter size, is determined it moves toward by Δt and generate the acceleration at time $t + \Delta t$.

Eq. (3.4) and the velocity are expressed in discretized form as follows

$$\bar{\mathbf{u}} = \mathbf{u} + \lambda \mathbf{L}_4 \mathbf{u}, \quad \mathbf{a} = \mathbf{L}_2 \mathbf{u}, \quad \mathbf{v} = \mathbf{L}_1 \mathbf{u} \tag{3.16}$$

where $\mathbf{L}_i$, $\bar{\mathbf{u}}$, $\mathbf{u}$, $\mathbf{v}$, $\mathbf{a}$ are the linear algebraic i^{th} difference operator matrix, the measured displacement, generated displacement, velocity, acceleration, respectively. $\mathbf{L}_4$ is order of $(2k+1) \times (2k+5)$, $\mathbf{L}_2$ and $\mathbf{L}_1$ are order of $(2k+1) \times (2k+3)$. Each operator matrix is expressed as Eq. (3.17-19). As finite differential operator is

17

used, one or two fictitious nodes are needed. The value of fictitious nodes is deter-mined by engineering sense, but barely affects the result.

$$\mathbf{L}_4 = \frac{1}{(\Delta t)^4} \begin{bmatrix} 1 & -4 & 6 & -4 & 1 & & & & \\ & 1 & -4 & 6 & -4 & 1 & & & 0 \\ & & & \ddots & & & & & \\ & 0 & & & 1 & -4 & 6 & -4 & 1 \\ & & & & & 1 & -4 & 6 & -4 & 1 \end{bmatrix} \qquad (3.17)$$

$$\mathbf{L}_2 = \frac{1}{(\Delta t)^2} \begin{bmatrix} 1 & -2 & 1 & & & \\ & 1 & -2 & 1 & & 0 \\ & & \ddots & & & \\ & 0 & & 1 & -2 & 1 \\ & & & 1 & -2 & 1 \end{bmatrix} \qquad (3.18)$$

$$\mathbf{L}_1 = \frac{1}{(2\Delta t)^2} \begin{bmatrix} 1 & 0 & 1 & & & \\ & 1 & 0 & 1 & & 0 \\ & & \ddots & & & \\ & 0 & & 1 & 0 & 1 \\ & & & 1 & 0 & 1 \end{bmatrix} \qquad (3.19)$$

Eq. (3.16) can be expressed as follows, including fictitious nodes.

$$\overline{\mathbf{u}} = \mathbf{u} + \lambda \mathbf{L}_4 \begin{bmatrix} \mathbf{u}^i \\ \mathbf{u} \\ \mathbf{u}^f \end{bmatrix} \quad \text{and} \quad \mathbf{L}_4 = \begin{bmatrix} \mathbf{L}_4^i & \mathbf{L}_4^c & \mathbf{L}_4^f \end{bmatrix} \qquad (3.20)$$

where $\mathbf{u}^i$, $\mathbf{u}^f$, $\mathbf{L}_4^i$, $\mathbf{L}_4^c$ and $\mathbf{L}_4^f$ are initial fictitious node, end fictitious node, operator matrix for each nodes, respectively. Since the fictitious nodes can have

18

zero values, Eq. (3.20) converts into:

$$\overline{\mathbf{u}} = (\mathbf{I} + \lambda\mathbf{L}_4^c)\mathbf{u} + \lambda\mathbf{L}_4^i\mathbf{u}^i + \lambda\mathbf{L}_4^f\mathbf{u}^f \rightarrow \mathbf{a} = \mathbf{L}_2(\mathbf{I} + \lambda\mathbf{L}_4^c)^{-1}\overline{\mathbf{u}} = \mathbf{C}^D\overline{\mathbf{u}} \qquad (3.21)$$

where $\mathbf{C}^D$ is the coefficient matrix for the acceleration generation of order $(2k+1) \times (2k+3)$. Superscript 'D' denotes the FDM method.

The acceleration at the center of a time window is the (k+2)-th component of $\mathbf{a}$ vector, a_{k+1}. It is considered as the generated acceleration at time t.

$$\begin{aligned}
a(t) = a_{k+1} &= \mathbf{c}^D\overline{\mathbf{u}}\frac{1}{(\Delta t)^2} = \frac{1}{(\Delta t)^2}\sum_{p=1}^{2k+1}C_{k+1,p}^D\overline{u}_p \\
&= \frac{1}{(\Delta t)^2}\sum_{p=-k}^{k}c_{p+k+1}^D\overline{u}(t+p\Delta t)
\end{aligned} \qquad (3.20)$$

where $\mathbf{c}^D$ denotes the center row of the $\mathbf{C}^D$ matrix. The Fourier transform of Eq. (3.20) yields the transfer function of the FDM-FIR filter, $H_D(f)$.

$$\begin{aligned}
F(a(t)) &= \frac{1}{(\Delta t)^2}\sum_{p=-k}^{k}c_{p+k+1}^D e^{i2\pi fp\Delta t}F(\overline{u}(t)) \\
H_D(f) &= \frac{1}{(\Delta t)^2}\sum_{p=-k}^{k}c_{p+k+1}^D e^{i2\pi fp\Delta t}
\end{aligned} \qquad (3.21)$$

where i is the imaginary unit. The transfer function of FDM-FIR filter approximates the original transfer function in discretized form given in Eq. (3.6)

$$H_{TF}(f) \approx \frac{1}{(\Delta t)^2} \sum_{p=-k}^{k} c_{p+k+1}^{D} e^{i2\pi f p \Delta t} \tag{3.22}$$

Eq. (3.22) illustrates the truncated Fourier series of the transfer function and the coefficients of the FDM-FIR filter are determined by following process.

$$
\begin{aligned}
c_{p+k+1}^{D} &= (\Delta t)^2 \frac{1}{f_s} \int_{f_s/2}^{f_s/2} H_{TF}(f) e^{-i2\pi f p \Delta t} df \\
&= (\Delta t) \int_{f_s/2}^{f_s/2} H_{TF}(f) e^{-i2\pi f p \Delta t} df
\end{aligned} \tag{3.23}
$$

where $f_s = 1/\Delta t$ stands for the sampling frequency of measurement. The transfer function $H_{TF}(f)$ is an even function. Thus the imaginary part of integrand diminishes by Euler's fornula.

$$
\begin{aligned}
c_{p+k+1}^{D} &= (\Delta t) \int_{f_s/2}^{f_s/2} H_{TF}(f) e^{-i2\pi f p \Delta t} df \\
&= -(\Delta t)^3 (2\pi)^2 \int_{f_s/2}^{f_s/2} \frac{f^2}{1+\lambda(2\pi f)^4} e^{-i2\pi f p \Delta t} df \\
&= -2(2\pi)^2 \frac{(\Delta t)^3}{f_T} \int_{0}^{1/(2\tilde{f}_T)} \frac{\tilde{f}^2}{1+(1/\alpha_T - 1)\tilde{f}^4} \cos(2\pi p \tilde{f}_T \tilde{f}) d\tilde{f}
\end{aligned} \tag{3.24}
$$

where $\tilde{f}_T = f_T / f_s$ denotes the target frequency to the sampling frequency (TSF) ratio. As the transfer function decreases very quickly for higher $\tilde{f}$, the integral in Eq.
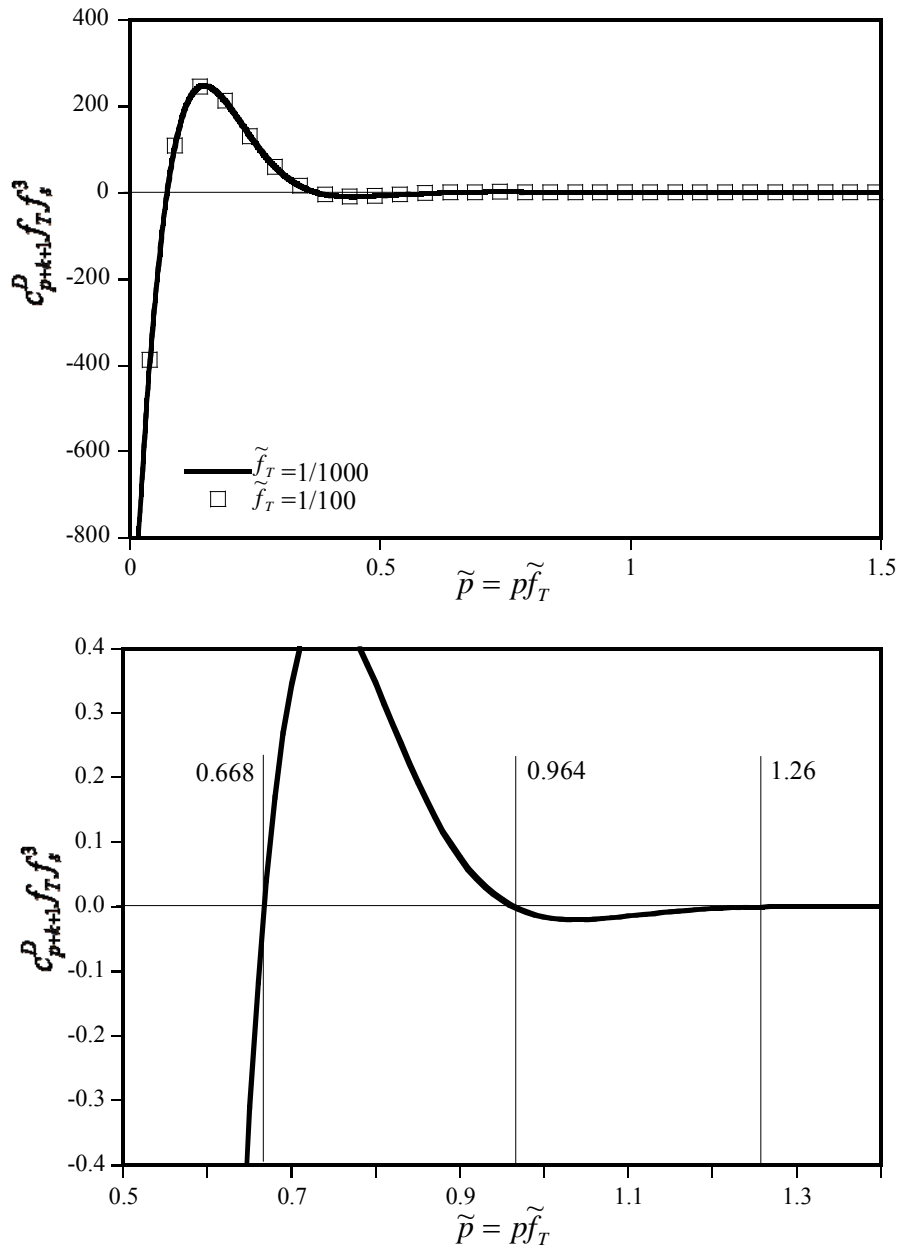
Fig. 3.4. Coefficients of the FDM-FIR filter:

(a) Small scale. (b) Detail in a large scale.

21

(3.26) is almost independent of small TSF ratio and thus becomes a function of $\tilde{p} = p\tilde{f}_T$ as shown in Fig 3.4(a). To avoid the rippling amplitude, the filter size should be chosen carefully. The zero-crossing points of the coefficients, as shown in Fig 3.4(b), must be selected to be the last term. The time window, i.e. in one filter size interval, has $2k+1$ measuring points inside which means it has $2\tilde{p}_0 / \tilde{f}_T + 1$ points.

The normalized transfer function and accuracy function of the FDM-FIR filter are derived as following equations.

$$\widetilde{H}_D(\tilde{f}) = -\frac{1}{(2\pi\tilde{f}_T)^2}(c_{k+1}^D + 2\sum_{p=1}^{k} c_{p+k+1}^D \cos(2\pi p\tilde{f}_T\tilde{f})) \qquad (3.25)$$

$$\widetilde{H}_D^{acc}(\tilde{f}) = -\frac{1}{(2\pi\tilde{f}_T\tilde{f})^2}(c_{k+1}^D + 2\sum_{p=1}^{k} c_{p+k+1}^D \cos(2\pi p\tilde{f}_T\tilde{f})) \qquad (3.26)$$

where $\widetilde{H}_D$ and $\widetilde{H}_D^{acc}$ are the normalized transfer function and accuracy function of the FDM-FIR filter, respectively. The FDM-FIR filter is capable of generating the velocity as well. Only the linear operator matrix is changed in this process. The normalized functions $\widetilde{H}_{D,v}$ and $\widetilde{H}_{D,v}^{acc}$ for the velocity generation:

$$\widetilde{H}_{TF,v}(\tilde{f}) = \frac{H_{TF,v}(f)}{i\omega_T} = \frac{1}{2\pi\tilde{f}_T}\sum_{p=1}^{k} c_{p+k+1}^c \sin(2\pi p\tilde{f}_T\tilde{f}) \qquad (3.25)$$

$$\widetilde{H}_{TF,v}^{acc}(\tilde{f}) = \frac{\widetilde{H}_{TF,v}(\tilde{f})}{\widetilde{H}_{E,v}(\tilde{f})} = \frac{1}{2\pi\tilde{f}_T\tilde{f}}\sum_{p=1}^{k} c_{p+k+1}^c \sin(2\pi p\tilde{f}_T\tilde{f}) \qquad (3.26)$$
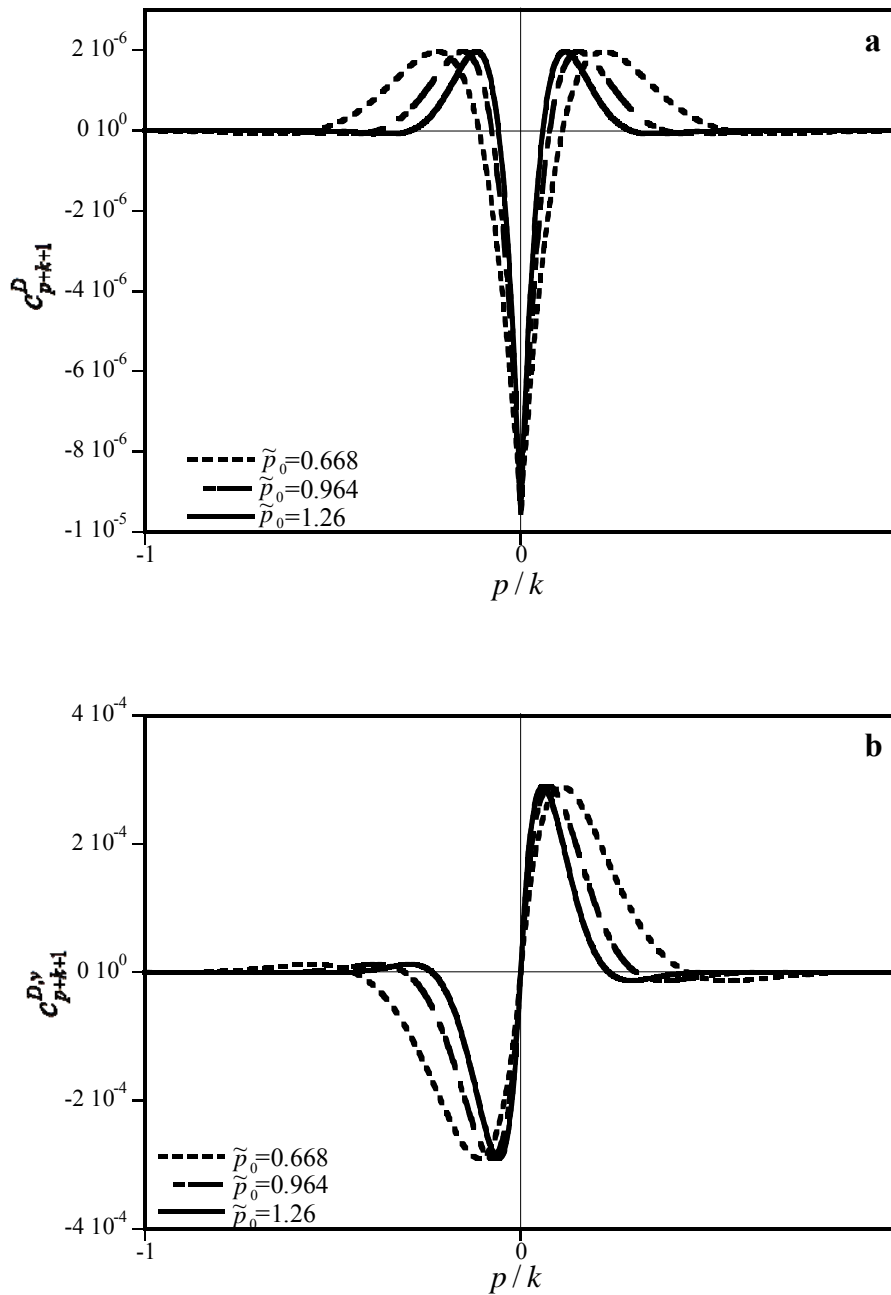
Fig. 3.5. Coefficients of the FDM-FIR filter for different filter size:

(a) Acceleration generation. (b) Velocity generation
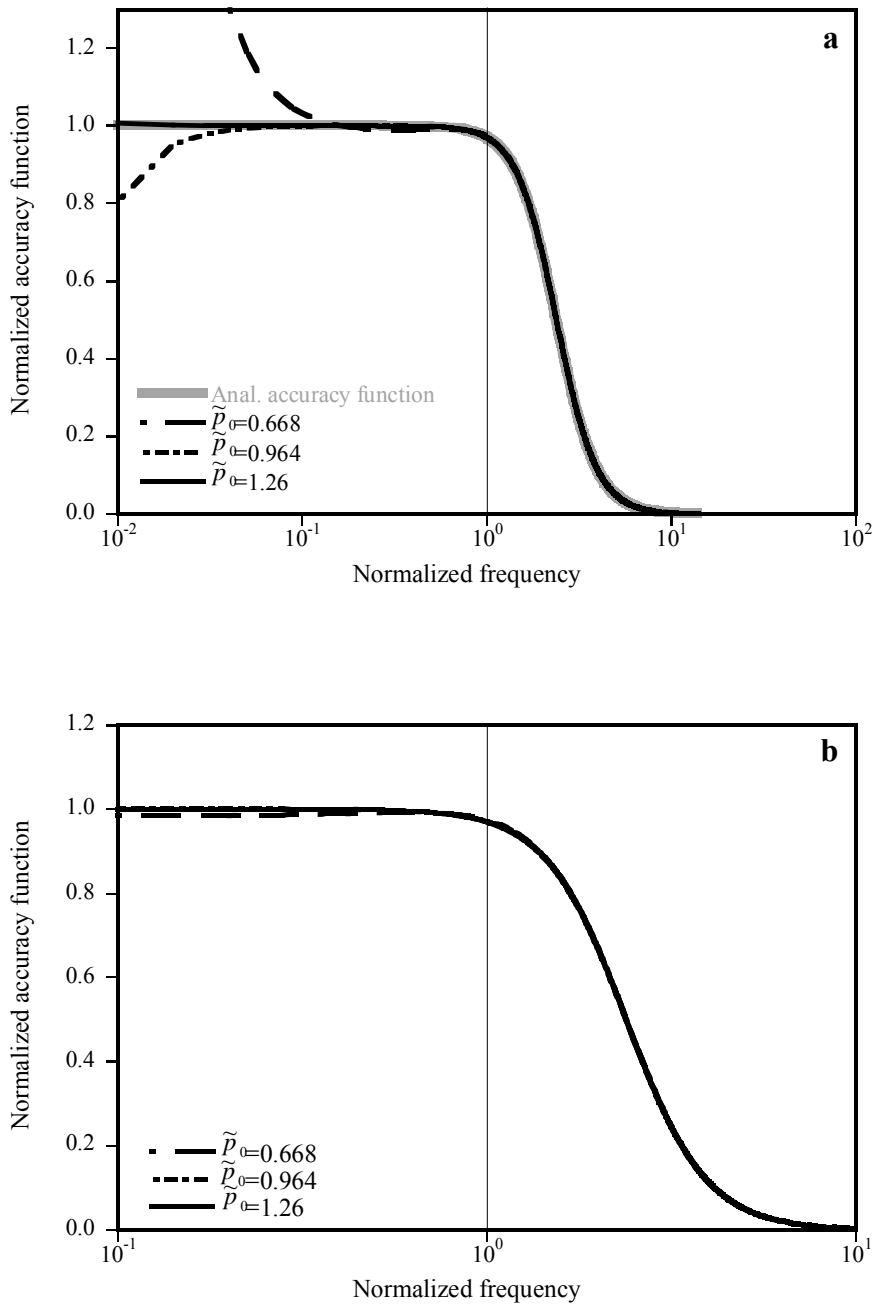
Fig. 3.6. Accuracy functions of the FDM-FIR filter for different filter size:

(a) Acceleration generation. (b) Velocity generation

24
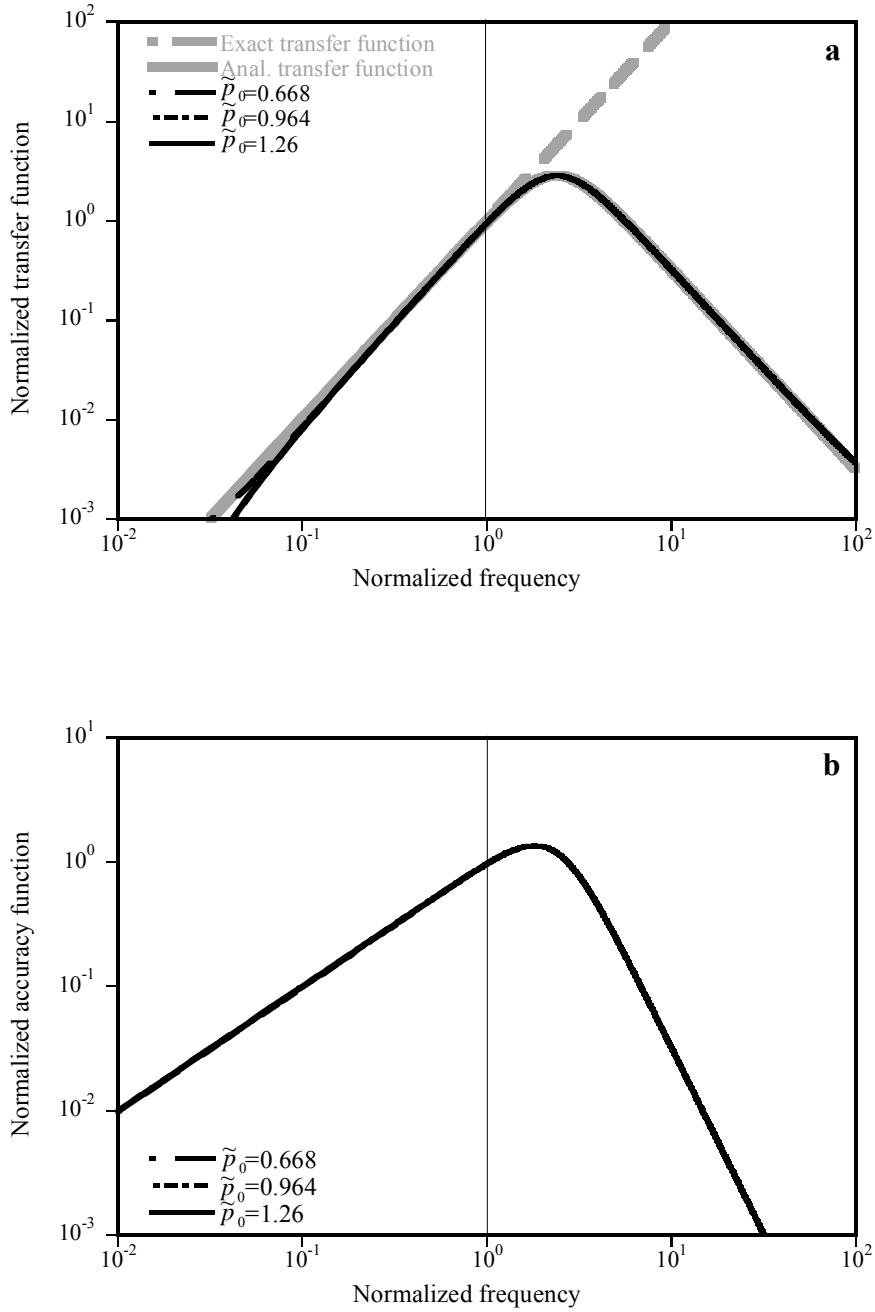
Fig. 3.7. Transfer functions of the FDM-FIR filter for different filter size:

(a) Acceleration generation. (b) Velocity generation

The coefficients, accuracy functions and transfer functions of the FDM-FIR filter for TSF ratio of 1/500 are presented in Fig. 3.5. through Fig. 3.7.. Regardless of the filter size, transfer functions approximates the analytic transfer function very well except for very low frequency section.

As shown in Fig. 3.6(a), long filter size guarantees accurate approximation of the transfer function. There is a trade-off that long filter size causes loss of information and increase of calculation time. Since the given problem does not need real-time generation of acceleration and velocity, measuring time can extended as needed and calculation time is not major problem. Once the information is generated and the flutter derivatives are evaluated, no further analysis on generating information is not needed. Thus long filter size of $\tilde{p}_0 = 1.26$ is used for the analysis in this paper.

3.2. Equation Error Estimator (EEE)

Once the full history of displacement is acquired, velocity and acceleration can be calculated by FDM-FIR filter, which will be dealt with in the next section. With full information the unknown system parameters can be extracted by EEE through the minimization process. The EEE gives convenient tool to the force controlled test which is hard to process with sensitivity analysis or eigenvalue analysis.

The EEE method minimizes the equation error of the dynamic system involving the unknown system parameters, which is the flutter derivatives for this research. To make this process clear, separate the known portion and the unknown portion of Eq. (2.13).

$$\mathbf{F}_{kn}(t_i) = \mathbf{F}_{ex}(t_i) - \mathbf{M}\ddot{\mathbf{u}}(t_i) \tag{3.27}$$

$$\mathbf{F}_{un}(\mathbf{X}, t_i) = \mathbf{C}_{eff}\dot{\mathbf{u}}(t_i) + \mathbf{K}_{eff}\mathbf{u}(t_i) = \mathbf{s}(t_i)\mathbf{X} \tag{3.28}$$

where subscripts '*kn*' and '*un*' indicates known and unknown portion, **s** is a sensitivity matrix consists of displacement and velocity for each time step t_i and **X** is the matrix which is composed of unknown parameters. **s** and **X** are defined as follows:

$$\mathbf{s}(t_i) = \begin{bmatrix} \dot{h}_1(t_i) & \dot{\alpha}_1(t_i) & h_1(t_i) & \alpha_1(t_i) & 0 & 0 & 0 & 0 \\ 0 & 0 & 0 & 0 & \dot{h}_1(t_i) & \dot{\alpha}_1(t_i) & h_1(t_i) & \alpha_1(t_i) \\ \dot{h}_2(t_i) & \dot{\alpha}_2(t_i) & h_2(t_i) & \alpha_2(t_i) & 0 & 0 & 0 & 0 \\ 0 & 0 & 0 & 0 & \dot{h}_2(t_i) & \dot{\alpha}_2(t_i) & h_2(t_i) & \alpha_2(t_i) \end{bmatrix} \tag{3.29}$$

$$\mathbf{X} = \begin{pmatrix} c_{11} & c_{12} & k_{11} & k_{12} & c_{21} & c_{22} & k_{21} & k_{22} \end{pmatrix}^{\mathrm{T}} \tag{3.30}$$

where subscript 1 and 2 denotes each test and components of $\mathbf{X}$ represents elements of effective damping and stiffness matrices.

Minimizing the equation errors for entire time history using L_2-norm makes given problem quadratic since the equation is linear with respect to the unknown system parameter.

$$\underset{\mathbf{X}}{\mathrm{Min}}\,\Pi(\mathbf{X}) = \frac{1}{2}\sum_{i=1}^{nt}\left\|\mathbf{F}_{un}(\mathbf{X},t_i) - \mathbf{F}_{kn}(t_i)\right\|_2^2 \tag{3.31}$$

Substitution of Eq. (3.28) into Eq. (3.31) results in following equation.

$$\begin{aligned}
\underset{\mathbf{X}}{\mathrm{Min}}\,\Pi(\mathbf{X}) &= \frac{1}{2}\sum_{i=1}^{nt}(\mathbf{F}_{un}(\mathbf{X},t_i) - \mathbf{F}_{kn}(t_i))^{\mathrm{T}}\cdot(\mathbf{F}_{un}(\mathbf{X},t_i) - \mathbf{F}_{kn}(t_i)) \\
&= \frac{1}{2}\mathbf{X}^{\mathrm{T}}\mathbf{S}\mathbf{X} - \mathbf{X}^{\mathrm{T}}\mathbf{G} + \frac{1}{2}\sum_{i=1}^{nt}\mathbf{F}_{kn}^{\mathrm{T}}(t_i)\mathbf{F}_{kn}(t_i)
\end{aligned} \tag{3.32}$$

where $\mathbf{S}$ and $\mathbf{G}$ are global sensitivity matrix and gradient vector and represented as follows

$$\mathbf{S} = \sum_{i=1}^{nt}\mathbf{s}^{\mathrm{T}}(t_i)\mathbf{s}(t_i),\quad \mathbf{G} = \sum_{i=1}^{nt}\mathbf{s}^{\mathrm{T}}(t_i)\mathbf{F}_{kn}(t_i) \tag{3.33}$$

The solution of Eq. (3.32) can be simply attained by solving linear algebraic equation owing to its linearity about the unknown parameters.

$$\frac{\partial \Pi(\mathbf{X})}{\partial \mathbf{X}} = \mathbf{SX} - \mathbf{G} = 0 \rightarrow \mathbf{X} = \mathbf{S}^{-1}\mathbf{G} \qquad (3.34)$$

A unique solution is always determined without iterations or complex analysis. The solution converges as long as the information measured in sufficient length of time is provided. Also EEE does not affected by initial conditions which usually bring errors to OEE.

3.3 Bias Check of L$_2$-Norm EEE

Measuring the motion of the section model inevitably involves noise. Elimination of noise is impossible, only suppression is probable method. Since the EEE used in extraction of flutter derivatives in formed with L$_2$-norm, equation must be squared for making quadratic problem. Usually, as observation time increases the noise included in measured information. Noises which has mean value of zero diminishes as long length data is summed. However, in this problem, measured displacement is squared in the process of EEE and the included error is squared as well. Squared error has positive value and long range of time only cumulates error only to be bias. Eq. (3.31) is in extended form as follows

$$\text{Min} \Pi = \frac{1}{2} \sum_t \left\| (\ddot{\mathbf{u}}_{exact}^t + \ddot{\mathbf{u}}_{error}^t)\mathbf{m} + (\mathbf{s}_{exact}^t + \mathbf{s}_{error}^t)\mathbf{X} - \mathbf{F}_{ex}^t \right\|_2^2 \qquad (3.35)$$

where $\mathbf{m}$, $\ddot{\mathbf{u}}_{exact}^t$, $\ddot{\mathbf{u}}_{error}^t$, $\mathbf{s}_{exact}^t$ and $\mathbf{s}_{error}^t$ are the mass vector, exact acceleration, error in measured acceleration, exact sensitivity matrix and error in sensitivity matrix, respectively. Partial differentiation of Eq. (3.35) with respect to $\mathbf{X}$ yields following equation

$$\frac{\partial \Pi}{\partial \mathbf{X}} = \sum_t \left[(\mathbf{s}_{exact}^t + \mathbf{s}_{error}^t)^T \left[(\ddot{\mathbf{u}}_{exact}^t + \ddot{\mathbf{u}}_{error}^t)\mathbf{m} + (\mathbf{s}_{exact}^t + \mathbf{s}_{error}^t)\mathbf{X} - \mathbf{F}_{ex}^t \right] \right]$$

$$= \sum_t \left[\begin{array}{l} (\mathbf{s}_{exact}^t + \mathbf{s}_{error}^t)^T (\ddot{\mathbf{u}}_{exact}^t + \ddot{\mathbf{u}}_{error}^t)\mathbf{m} \\ + (\mathbf{s}_{exact}^t + \mathbf{s}_{error}^t)^T (\mathbf{s}_{exact}^t + \mathbf{s}_{error}^t)\mathbf{X} - (\mathbf{s}_{exact}^t + \mathbf{s}_{error}^t)^T \mathbf{F}_{ex}^t \end{array} \right]$$

$$= \sum_t \left[\begin{array}{l} (\underbrace{\mathbf{s}_{exact}^{t}{}^T \ddot{\mathbf{u}}_{exact}^t}_{Exact\,term} + \underbrace{\mathbf{s}_{exact}^{t}{}^T \ddot{\mathbf{u}}_{error}^t + \mathbf{s}_{error}^{t}{}^T \ddot{\mathbf{u}}_{exact}^t}_{Cross\,Term} + \underbrace{\mathbf{s}_{error}^{t}{}^T \ddot{\mathbf{u}}_{error}^t}_{Error\,Term})\mathbf{m} \\[2em] + (\underbrace{\mathbf{s}_{exact}^{t}{}^T \mathbf{s}_{exact}^t}_{Exact\,Term} + \underbrace{\mathbf{s}_{exact}^{t}{}^T \mathbf{s}_{error}^t + \mathbf{s}_{error}^{t}{}^T \mathbf{s}_{exact}^t}_{Cross\,Term} + \underbrace{\mathbf{s}_{error}^{t}{}^T \mathbf{s}_{error}^t}_{Error\,Term})\mathbf{X} \\[2em] - (\underbrace{\mathbf{s}_{exact}^t}_{Exact\,Term} + \underbrace{\mathbf{s}_{error}^t}_{Error\,Term})^T \mathbf{F}_{ex}^t \end{array} \right] \qquad (3.36)$$

In matrix form, Eq. (3.28) becomes:

$$\begin{aligned} \frac{\partial \Pi}{\partial \mathbf{X}} &= \mathbf{M}_{Exact} + \mathbf{M}_{Cross} + \mathbf{M}_{Error} \\ &+ (\mathbf{S}_{Exact} + \mathbf{S}_{Cross} + \sigma_\mathbf{s}^2 \mathbf{S}_{Error})\mathbf{X} - (\mathbf{F}_{ex,Exact} + \mathbf{F}_{ex,Error}) = 0 \end{aligned} \qquad (3.37)$$

where σ_s is standard deviation of the error included in the sensitivity matrix and subscript '*Cross*' stands for the multiplication of exact term and error term. *Cross* terms diminishes as time cumulates but '*Error*' terms does not disappear. Thus extracted flutter derivatives might be 'shifted' from the exact flutter derivatives. Bias effect can be eliminated only if the characteristic values of error should be known, which is impossible to achieve.

To avoid this effect of bias, L_1-norm EEE is tested. Optimization equation for L_1-norm EEE is as follows

$$\text{Min}\Pi = \sum_t \left\| (\ddot{\mathbf{u}}_{exact}^t + \ddot{\mathbf{u}}_{error}^t)\mathbf{m} + (\mathbf{s}_{exact}^t + \mathbf{s}_{error}^t)\mathbf{X} - \mathbf{F}_{ex}^t \right\| \qquad (3.38)$$

Simplex is generally used for linear programming algorithm and it targets nonnegative variables. Therefore the algorithm need to be modified and an improved algorithm for L_1-norm optimization by Barrodale et al. (1973) is implemented for bias check test.

The EEE methods is applied to numerically simulated time-domain data of the section model. To acquire data, the flutter derivatives of the rectangular section which has width to depth ratio of 5 presented by Park et al. (2014) is used. The flutter derivatives are modified to satisfy causality condition and the analytic motion response is generated by the virtue of the Fourier series approximation (FSA) proposed by Park et al. (2014). The information obtained through force controlled test carried out in the wind tunnel necessarily contains error but acquired analytic solution is noise free and both EEE methods yields same result out of it, which is referred as the exact flutter derivatives.
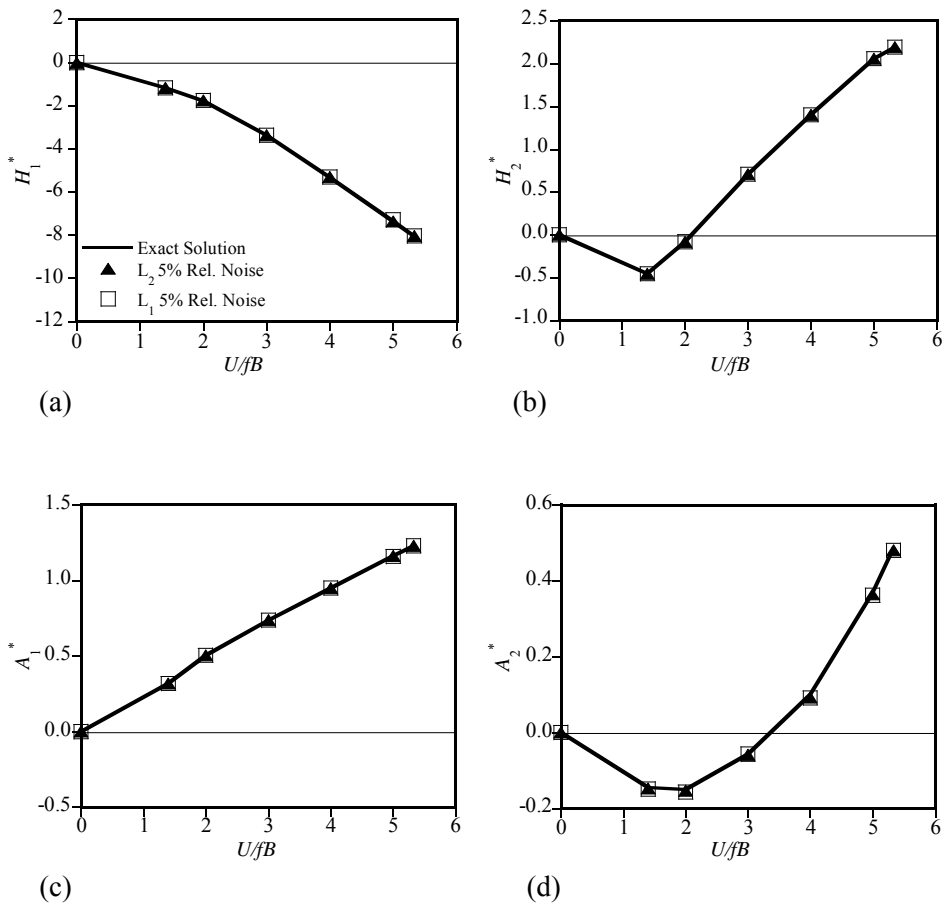
Fig. 3.8. Identified flutter derivatives for the rectangular section – damping coeffi-

cients: (a) H_1^* (b) H_2^* (c) A_1^* (d) A_2^*
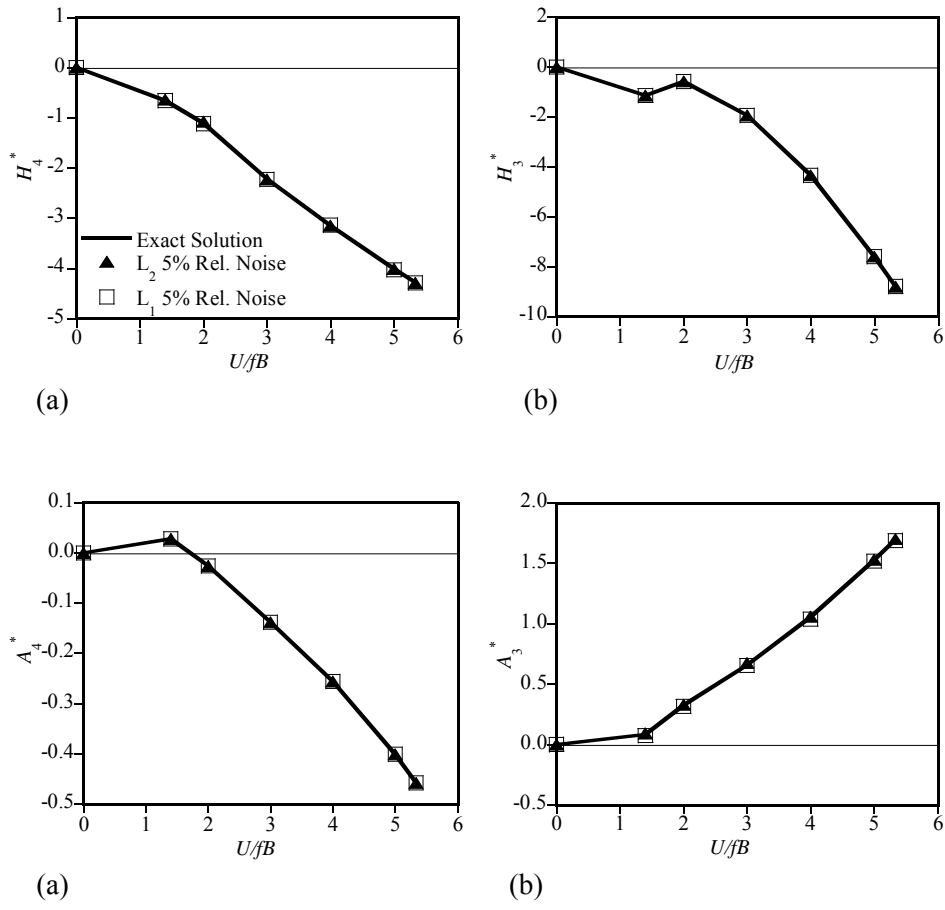
Fig. 3.9. Identified flutter derivatives for the rectangular section – stiffness coeffi-

cients: (a) H_4^* (b) H_3^* (c) A_4^* (d) A_3^*

To verify the effect of bias, relative random noise is applied to simulated time-domain displacement with amplitude of 5%. The velocity and acceleration is generated by FDM-FIR filter, which compresses the error. The displacement, velocity, acceleration, exciting force is implemented to L_1-norm EEE and L_2-norm EEE to compare the results. L_1-norm EEE takes longer computing time than L_2-norm EEE and from the characteristic feature of the simplex algorithm, the result can be blunder when the error is large.

As shown in Fig. 3.8. and Fig. 3.9., both EEE method yields nearly identical flutter derivatives. FDM-FIR filter has regularization scheme inside, as shown in Eq. (3.2). This regularization prevents the error from amplification when velocity and acceleration is generated. The effect of bias is negligible when error amplification is small, especially the given problem is about sinusoidal motion in single oscillating frequency. Since L_2-norm EEE has advantage of computing time and smoothing feature over L_1-norm EEE, this paper utilize L_2-norm EEE throughout the verification of the force controlled forced vibration test.

4. Applications and Verification
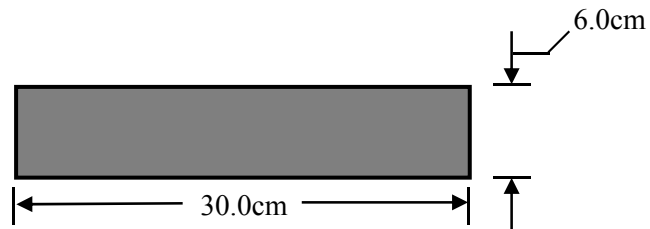
(a)
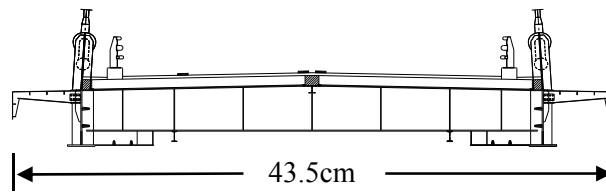
(b)

Fig. 4.1. Dimension of cross-section used in the test:

(a) a rectangular section. (b) Jido-bridge section

The Force controlled forced vibration test is applied to extract flutter derivatives of two bluff sections shown in Fig. 4.1. and to perform aeroelastic time domain analysis and frequency domain analysis with extracted flutter derivatives. The first section model, a rectangular section with a B/D ratio of 5, is typical case of bluff section which is often implemented in wind tunnel test for its complex behavior. The second section is the section model of Jido bridge, which is not more bluff than the first section. However, cross-DOF force analysis using the flutter derivatives extracted through the displacement controlled test indicates that Jido bridge section has severely complex wind-motion interaction.

All tests including the displacement controlled test, the force controlled test and free vibration test conducted using the wind tunnel, Le Cachalot at Seoul National University, Korea. Each section model is suspended on elastic springs to record its motion. Measured information can be compared to the time domain aeroelastic analysis. Four noncontact displacement meters measures motion of every corner of the section model and simple analytic process turns measurements into 2-DOF motion of the section models. Velocity and acceleration is generated by FDM-FIR filter and divided by its target accuracy to restore precision. Exciting force is applied by four motors, and force imposed on the section model is not measured during the test but curing prior test that assures exact imposition of force with detached metal guide. The mechanical properties of the rectangular section and Jido bridge section are presented in Table. 4.1. The first-order derivatives of the lift coefficient, C_L, and moment coefficient, C_M, with respect to the attack angle are given in Table 4.2. These parameters

are used for FSA and complex eigenvalue analysis to evaluate flutter velocity. The sign convention for torsional displacement and moment force is assumed to be positive for the nose-up direction.

Table 4.1. Mechanical properties concerning the systems used in the examples

		Rectangular section	Jido bridge section
Masses	m_h (kg/m)	5.902	3.640
	m_α (kg $\cdot$ m^2/m)	0.229	0.102
Damping ratio	c_h (kg/s/m)	1.626	1.003
	c_α (kg $\cdot$ m^2/s/m)	0.064	0.022
Frequencies	f_h (Hz)	3.05	3.05
	f_α (Hz)	6.68	5.13

Table 4.2. First-order derivatives of the lift and moment coefficients

Type of section	$\left.\dfrac{\partial C_L}{\partial \vartheta}\right|_{\vartheta=0}$	$\left.\dfrac{\partial C_M}{\partial \vartheta}\right|_{\vartheta=0}$
Rectangular section	7.65	-0.77
H-type section	4.31	0.93

4.1 Rectangular Section of B/D=5

The flutter derivatives extracted from the EEE does not satisfy the causality condition, thus need to be modified by FSA. Fig. 4.2. and Fig. 4.3. show the flutter derivatives representing aeroelastic damping ratio and stiffness, respectively. The flutter derivatives obtained by the displacement controlled test and the force controlled test are drawn together with unmodified flutter derivatives. Exciting force of the force controlled test and oscillating frequency of the displacement controlled test are 2.5Hz. It is selected based on the vertical and torsional natural frequency, since medium value of both frequency yields equal level of response. The results from two different test methods are almost identical in low non-dimensional wind velocity but slightly different in high dimensionless wind velocity section, However, the difference is small. The causality condition of flutter derivatives are properly satisfied when extracted, since only modest difference are observed with or without causality.

Modified flutter derivatives are utilized in aeroelastic analysis. From frequency domain aeroelastic analysis using SMA (Jung et al. 2014), flutter velocity is estimated to be 5.88m/s for the displacement controlled test and 5.19m/s for the force controlled test. Both results and change of system torsional system damping is depicted in Table. 4.3. and Fig. 4.4. In actual wind tunnel test, the flutter velocity for the rectangular section is observed to be in the range from 5.00m/s to 5.20m/s. From the result, it can be said that the force controlled test estimates the flutter velocity closely to the actual value. Time domain aeroelastic analysis is performed implementing FSA (Park et al. 2014). Measured wind tunnel data at the wind velocity of 5.13m/s is used, which is

39

obtained during the force controlled test. Time domain data at high wind velocity is impossible to attain since the system damping increases as wind speed goes up, however, exciting force makes the motion stays at steady-state so that reliable long time data can be recorded. The dimensionless wind velocity of this analysis is 6.84, which indicates the difference of two flutter derivatives at x-axis value of 6.84 in Fig. 4.2. and Fig. 4.3. makes difference in time domain analysis. The results are presented in Fig. 4.5-6 and both test method estimates the motion of section model well.
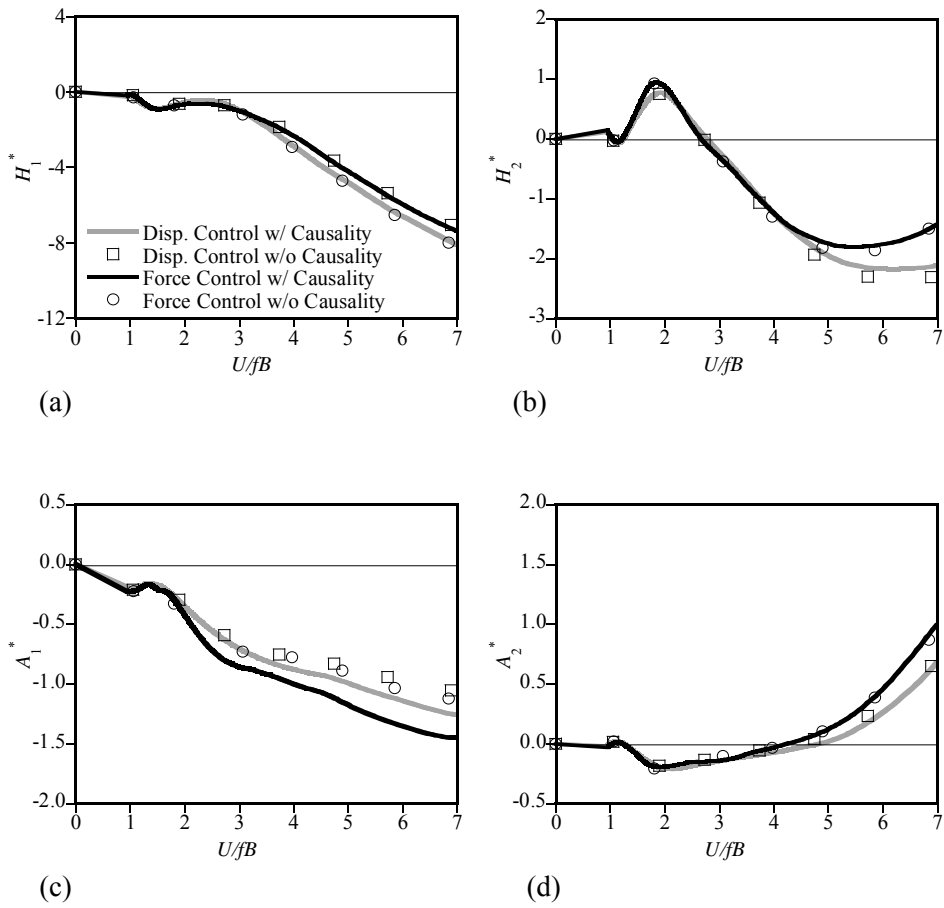
Fig. 4.2. Flutter derivatives of the rectangular section for the aerodynamic damping:

(a) H_1^* (b) H_2^* (c) A_1^* (d) A_2^*

41
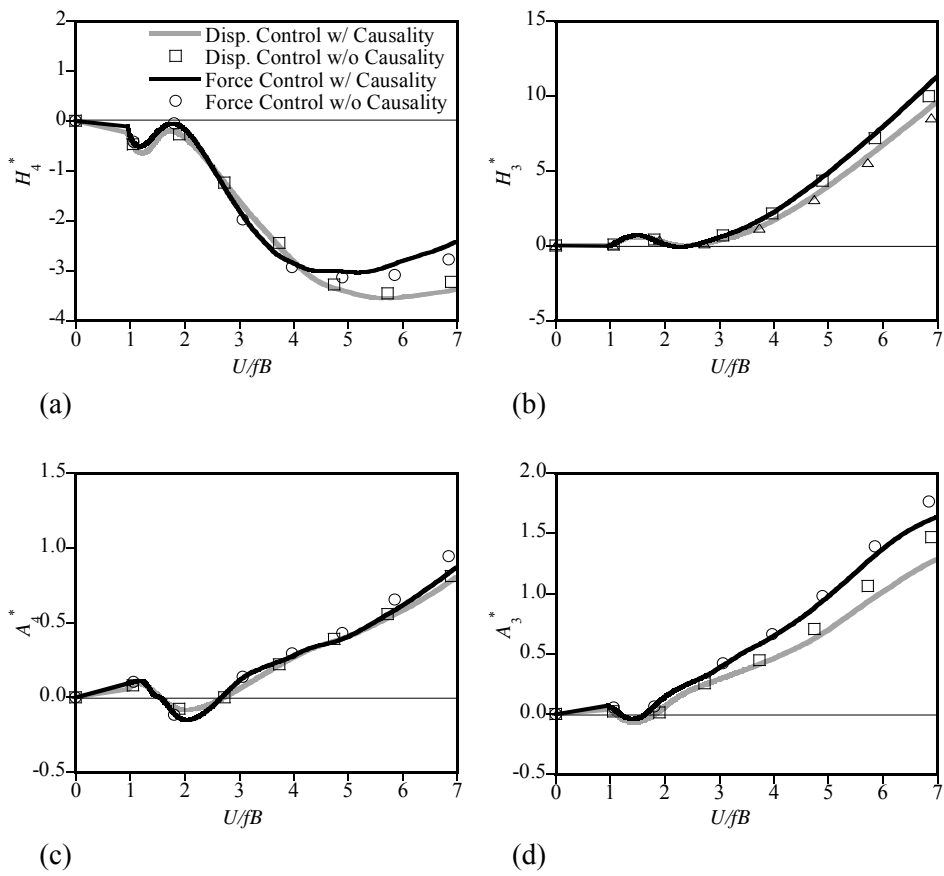
Fig. 4.3. Flutter derivatives of the rectangular section for the aerodynamic stiffness

(a) H_4^* (b) H_3^* (c) A_4^* (d) A_3^*

Table 4.3. Frequency domain aeroelastic analysis: a rectangular section

	Observation	Calculation	
	Wind tunnel	Displ. control	Force control
Flutter velocity, m/s	5.00 ~ 5.20	5.88	5.19
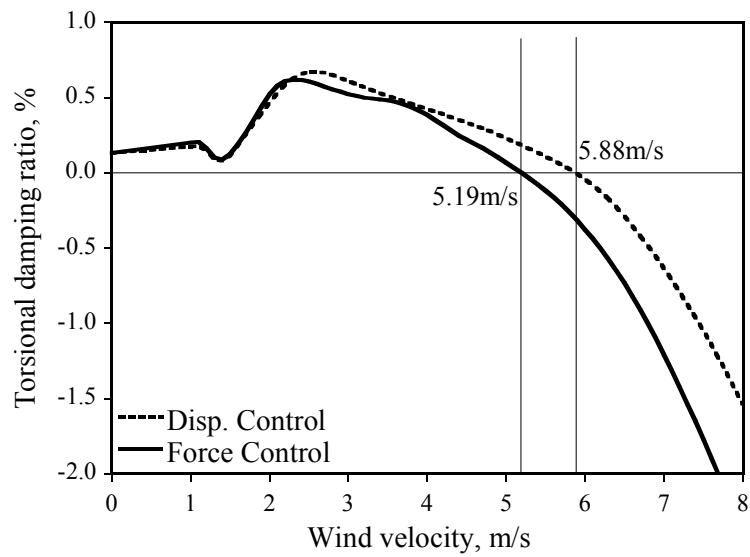
Fig. 4.4. Torsional system damping ratio for different test method of a rectangular

section
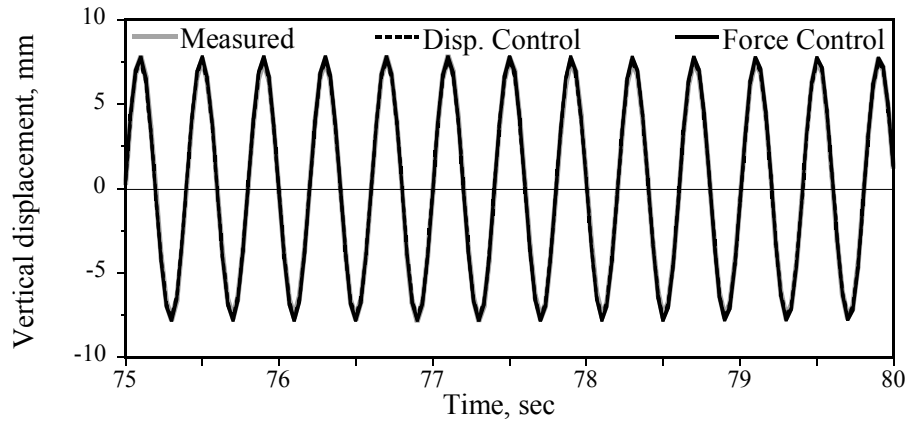
(a)
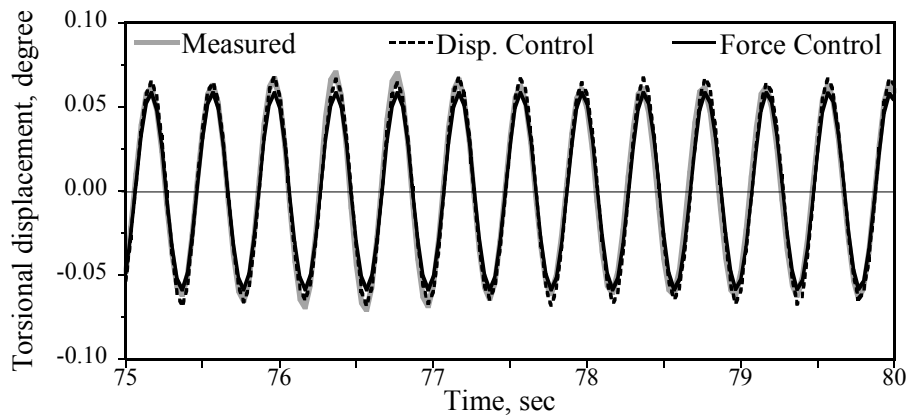
(b)

Fig. 4.5. Displacement estimation of rectangular section for different test methods:

Vertical excitation

(a) Vertical displacement. (b) Torsional displacement
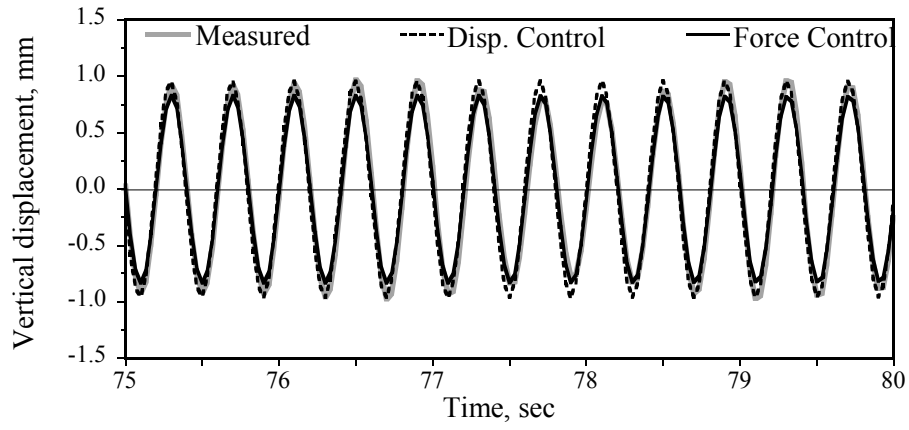
(a)
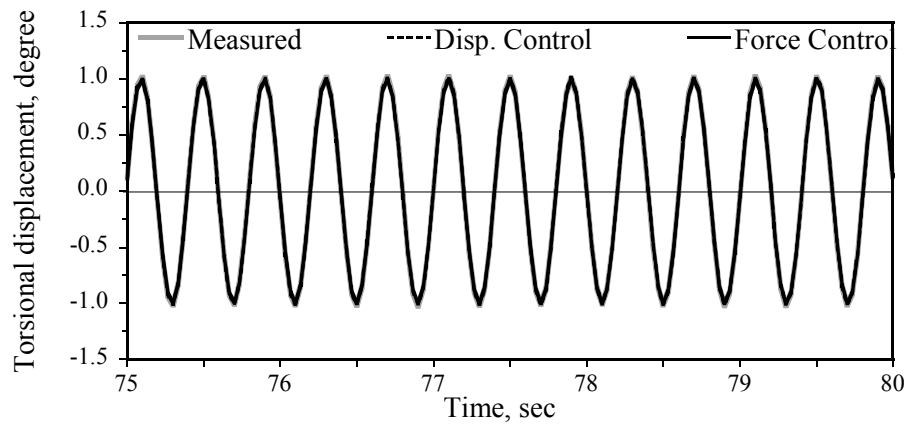
(b)

Fig. 4.6. Displacement estimation of rectangular section for different test methods:

Torsional excitation

(a) Vertical displacement. (b) Torsional displacement

4.2 Jido Bridge Section

Same tests are conducted to Jido bridge section with the same experimental setup. This section model has flaps on both side which alleviates the vortex induced vibration (VIV). Natural frequencies of the section model are set to be close, ratio of 1.6. As excitation frequency got close to the natural frequency, response level will be maximize and the interaction between the motion and wind can be observed clearly.

The flutter derivatives are shown in Fig. 4.7. and Fig. 4.8. Components show similar result for both test methods except for H_2^* and H_4^*. Modified H_2^* shows quite different tendency from the unmodified one in Fig. 4.7.. The difference of the force controlled test is larger than that of the displacement controlled test. It can be interpreted as the linear assumption of H_2^* violates causality condition considerably in the force controlled test. Same result can be seen in H_4^* in Fig. 4.8., but this time both test methods violates causality condition by similar amount.

Frequency domain aeroelastic analysis shows both methods estimate the flutter velocity well. Change of torsional damping ratio of the system is very similar and turns into negative value at very similar wind velocity. However, time domain aeroelastic analysis result is very different from that of the first section. Time domain data at wind velocity of 10.97m/s is utilized and the dimensionless velocity is 11.46. Estimation of displacement by both methods show similar results in Fig. 4.10. and Fig. 4.11., but different from the measured displacement. Especially cross-displacements such as torsional displacement of vertical excitation case and vertical displacement of

torsional excitation case. This large difference is may caused by assumption of the aeroelastic forces. Since the interaction between the motion and the force is complex for bluff sections with cables and rails, linear assumption is not sufficient to model aeroelastic forces.
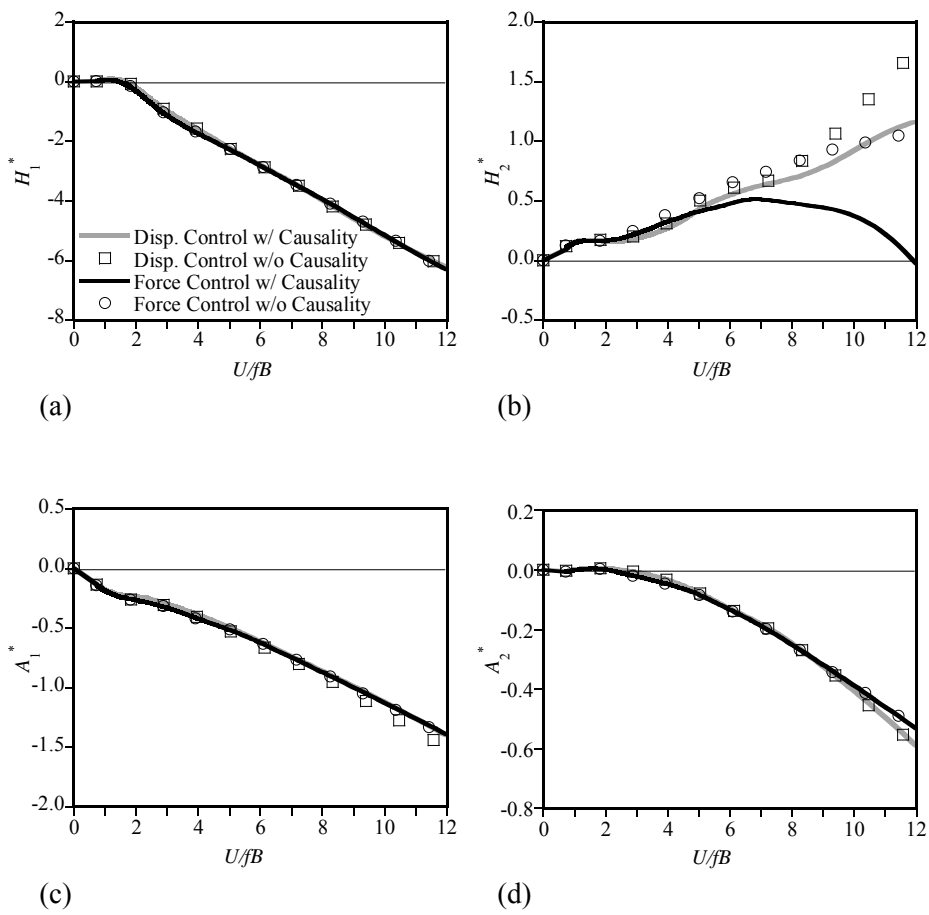
Fig. 4.7. Flutter derivatives of Jido bridge section for the aerodynamic damping:
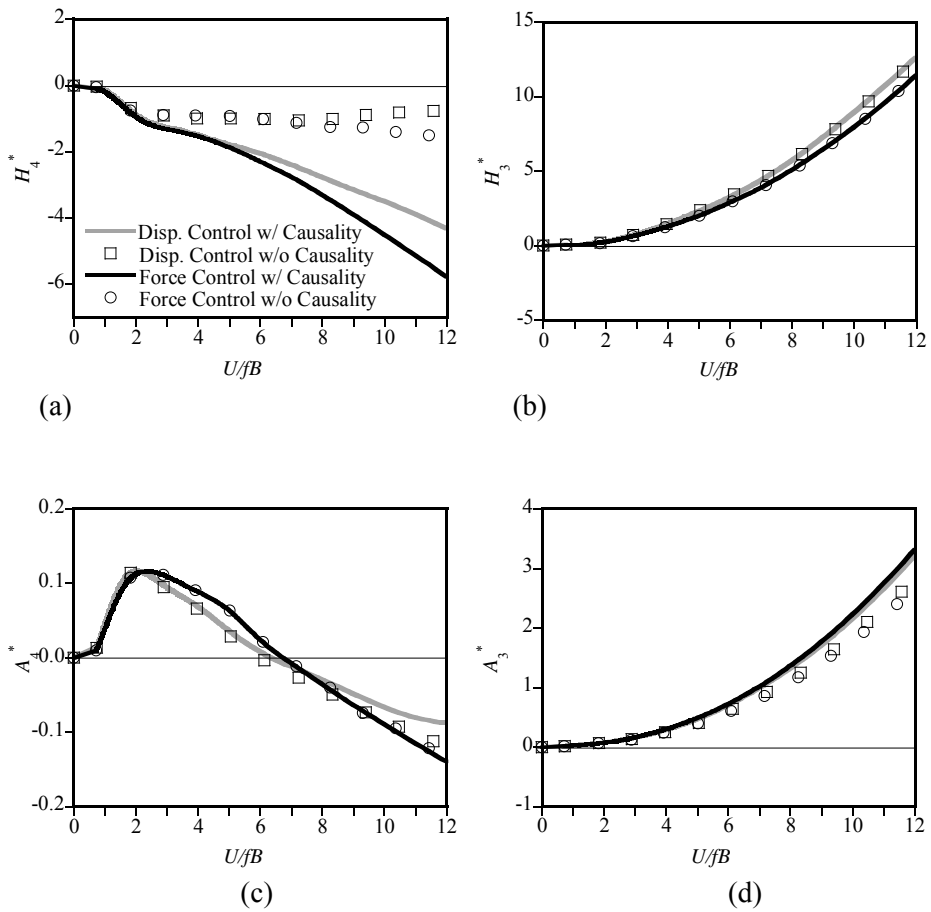
(a) H_1^* (b) H_2^* (c) A_1^* (d) A_2^*

Fig. 4.8. Flutter derivatives of Jido bridge section for the aerodynamic damping:

(a) H_1^* (b) H_2^* (c) A_1^* (d) A_2^*

Table 4.4. Frequency domain aeroelastic analysis: Jido bridge section

	Observation	Calculation	
	Wind tunnel	Displ. control	Force control
Flutter velocity, m/s	11.0 ~ 12.0	11.56	11.39
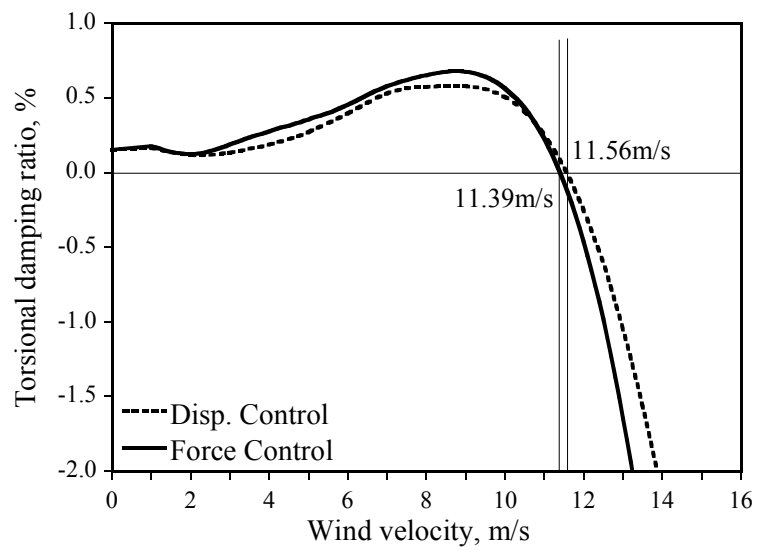
Fig. 4.9. Torsional system damping ratio for different test method of Jido bridge section
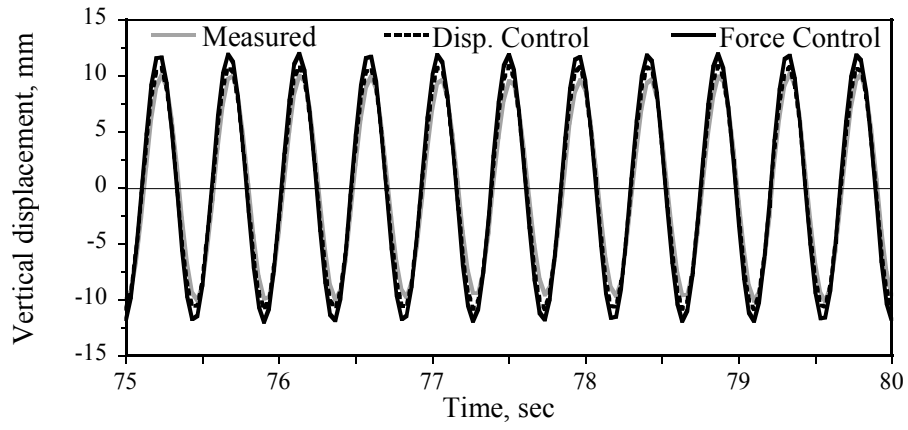
(a)
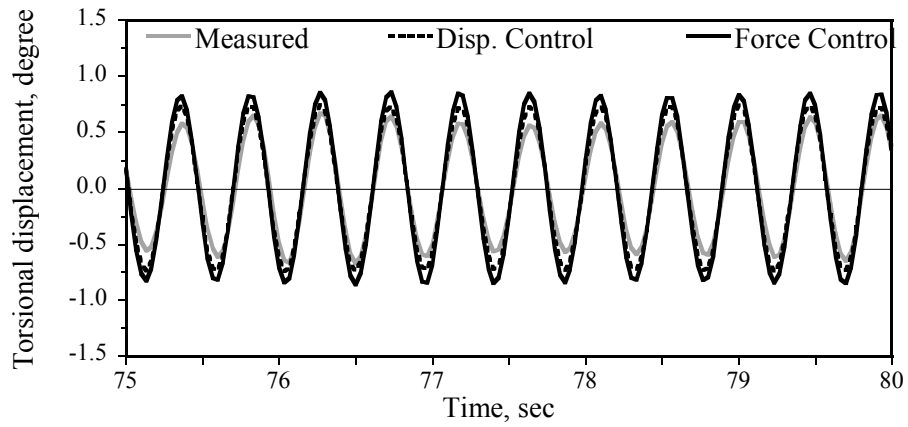
(b)

Fig. 4.10. Displacement estimation of Jido bridge section for different test methods:

Vertical excitation

(a) Vertical displacement. (b) Torsional displacement
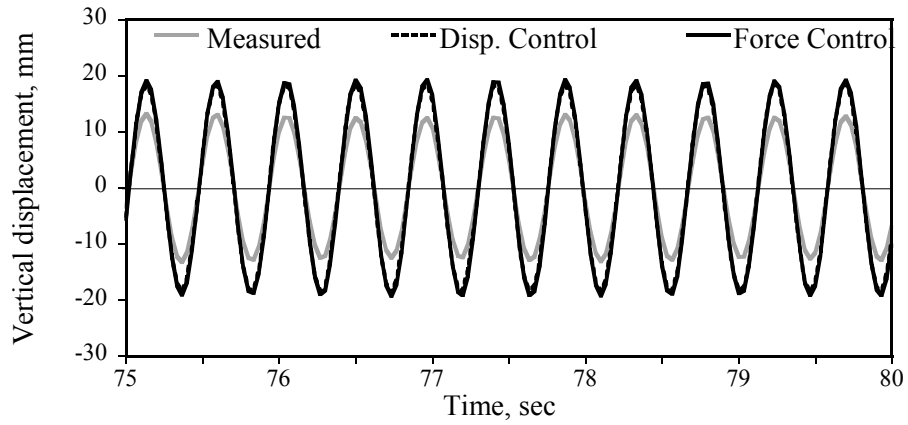
(a)
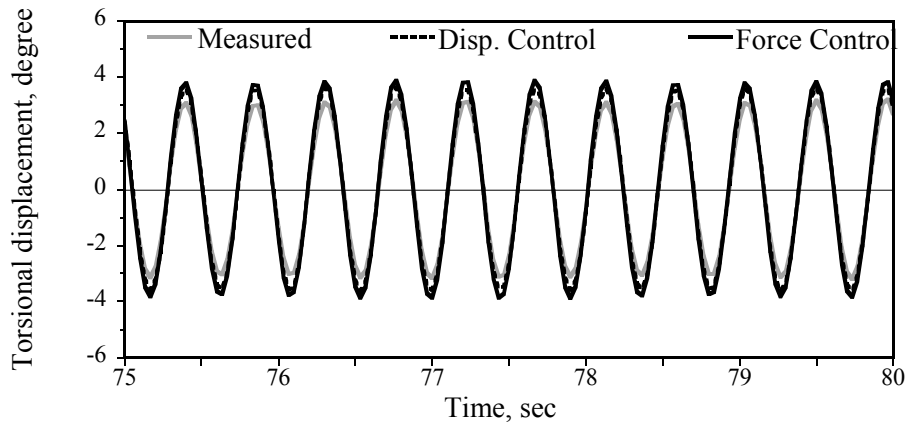
(b)

Fig. 4.11. Displacement estimation of Jido bridge section for different test methods:

Torsional excitation

(a) Vertical displacement. (b) Torsional displacement

51

5. Summary and Conclusions

A new technique to extract flutter derivatives is performed to consider complex interaction between the flow filed and the motion of a bridge. Freely suspended section model changes its motion as aeroelastic force is changed vice versa. This nonlinearity, which is ignored in conventional test method, is expected to bring difference to the flutter derivatives. The force controlled forced vibration test is simply designed to change input and output of the displacement controlled forced vibration test, however, extracting technique is very complex.

Equation error estimation (EEE) technique is introduced by Hong (2012) and EEE requires full history of information, which is hard to achieve by experimental instruments. FDM-FIR filter is introduced to generate velocity and acceleration from measured displacement and moving window technique is adopted for generation. Optimal window size and regularization factor is decided based on the work of Hong (2012). L_2-norm EEE has possibility for leaving bias to flutter derivatives when measured error is amplified as it goes through FDM-FIR filter, thus L_1-norm EEE is designed to check bias effect. The example implementing the mechanical properties from the work of Park et al. (2014) is examined and assured that the bias is negligible amount for given problem. And extracted flutter derivatives are modified by the Fourier series approximation (FSA) (Park et al., 2014) to satisfy its causality condition.

The force controlled test is conducted for two types of bridge section models, one

is typical bluff section, a rectangular section with B/D ratio of 5 and the other is real bridge section, Jido bridge section model. Frequency domain aeroelastic analysis over flutter derivatives estimated flutter onset velocity. Both methods evaluated similar velocity which is very close to the flutter velocity observed in wind tunnel test. Time domain information collected during the force controlled test is utilized for comparison with the time domain aeroelastic anlaysis result. For the rectangular section, both methods showed similar result and coincide with observed data. However, Jido bridge section resulted differently, both methods yield similar displacement data but different from observed one. Linear assumption for aeroelastic force violated the causality condition of the flutter derivatives severely in this section model. As long as the linear assumption for the aeroelastic forces is hold, the nonlinear effect of the interaction can be neglected for general bridge section model test.

REFERENCES

Barrodale (1973)

Barrodale, I. and Roberts, F. D. K. (1973). "An improved algorithm for discrete l_1 linear approximation" SIAM J. Numer. Anal. Vol. 10, No. 5, 839-848

Bartoli (2009)

Bartoli, G. Contri, S., Mannini, C. and Righi, M., "Toward an improvement in the identification of bridge deck flutter derivatives", *Journal of Engineering mechanics,* vol. 135 (8), 771-785

Chen (2004)

Chen, X. and Kareem, A., "Efficacy of the implied approximation in the identification of flutter derivatives", *Journal of Structural Engineering,* vol. 130(12), 2070-2074

Chowdhury (2003)

Chowdhury, A. G. and Sarkar, P. P., "A new technique for identification of eighteen flutter derivatives using a three-degree-of freedom section model", *Engineering Structures,* vol. 25(14), 1763-1772

Diana (2004)

Diana, G., Resta, F., Zasso, A., Belloli, M. and Rocchi, D., "Forced motion and free motion aeroelastic tests on a new concept dymometric section model of the Messina suspension bridge", *Journal of Wind Engineering and Industrial Aerodynamics,* vol. 92, 441-462

Falco (1992)

Falco, M., Curami, A. and Zasso, A., "Nonlinear effects in sectional model aeroelastic parameters identification", *Journal of Wind Engineering and Industrial Aerodynamics,* vol. 41-44, 1321-1332

Gu (2000)

Gu, M., Zhang, R. and Xiang, H., "Identification of flutter derivatives of bridge decks", *Journal of Wind Engineering and Industrial Aerodynamics*, vol. 84, 151–162

Hong (2012)

Hong, Y. H., "Reconstruction of dynamic displacement and velocity based on the variational statement of an inverse problem from measured acceleration with special application to the extraction of flutter derivatives", Unpublished doctoral dissertation, Seoul National University, Korea, 2012

Iwamoto (1995)

Iwamoto, M. and Fujino, Y., "Identification of flutter derivatives of bridge deck from vibration data", *Journal of Wind Engineering and Industrial Aerodynamics*, vol. 54/55, 55–63

Jung (2014)

Jung, K. J., Kim, H. K. and Lee, H. S. "New unified approach for aeroelastic analyses using approximate transfer functions of aerodynamic forces", *Journal of Engineering Mechanics,* vol. 140, No. 4, 04013002

Kim (2007)

Kim, J.D. and King, J.P.C., *The Development of Wind Tunnel Test Technique for an Aeroelastic Buffeting Analysis of Long-span Bridges*, BLWTL-SS19-2007-DRAFT Report submitted to Korea Wind Engineering Research Center, The Boundary Layer Wind Tunnel Laboratory of The University of Western Ontario, (2007).

Li (2003)

Li, Y., Liao, H. and Qiang, S., "Weighting ensemble least-square method for flutter derivatives of bridge decks", *Journal of Wind Engineering and Industrial Aerodynamics,* vol. 91, 713–721

Matsumoto (1993)

Matsumoto, M., Shiraishi, N., Shigetaka, K. and Niihara, Y., "Aerodynamic derivatives of coupled/hybrid flutter of fundamental structural sections", *Journal of Wind Engineering and Industrial Aerodynamics*, vol. 49, 575–584

Park (2014)

Park, J. W., Jung, K. J., Hong, Y. H., Kim, H. K. and Lee, H. S., "Exact enforcement of the causality condition on the aerodynamic impulse response function using a truncated Fourier series", *Journal of Engineering Mechanics,* vol. 140, No. 5, 04014017

Sarkar (1992)

Sarkar, P. P., Jones, N. P. and Scanlan, R. H., "System identification for estimation of flutter derivatives", *Journal of Wind Engineering and Industrial Aerodynamics*, vol. 41/44, 1243–1254

Sarkar (1994)

Sarkar, P. P., Jones, N. P. and Scanlan, R. H., "Identification of aeroelastic parameters of flexible bridges", *Journal of Engineering Mechanics*, ASCE, vol. 120(8), 1718– 1741

Scanlan (1971)

Scanlan, R. H. and Tomko, J. J., "Airfoil and bridge deck flutter derivatives",

Journal of Engineering Mechanics Division, ASCE, vol. 97 (6), 1717–1733

초 록

이 연구에서는 단면의 움직임과 공기력의 상호작용에 의한 비선형성을 반영할 수 있고, 움직임의 정상상태 유지가 가능한 새로운 실험인 하중제어 강제가진 실험을 통해 플러터 계수를 추출한다. 기존의 실험 방법인 변위제어 강제가진 실험에서 플러터 계수를 추출하는 데에 사용된 MITD, ULS 그리고 해석해 등의 방법이 적용되기 힘들기 때문에 Equation error estimation (EEE) 가 이용되고, 이 때에 변위뿐만 아니라 속도와 가속도가 필요하게 된다. 이러한 정보를 생성하기 위해 움직이는 시간창 기법이 적용된 FDM-FIR 필터가 이용되고, 최적의 창 크기와 정규화 계수를 구하게 된다. EEE 기법에 사용되는 L_2-nom의 경우 측정된 오차가 필터를 통과하며 증폭될 시에 증폭된 오차가 제곱되어 편향성 문제를 일으킬 가능성이 있기에 편향성이 발생하지 않는 L_1-norm EEE를 구성하여 기존의 알려진 단면에 대한 예제를 수행한 결과 오차의 증폭량이 크지 않아 편향성의 크기가 매우 작기 때문에 L2-norm을 사용하였다. 새로운 실험의 타당성은 두 개의 단면에 대해 검증되었는데 폭-깊이 비 5의 직사각형 단면과 지도대교 단면에 대해 실험이 수행되었다. 추출된 플러터 계수가 Causality condition을 만족하도록 수정한 뒤 주파수영역 공탄성 해석을 실시해 플러터 풍속을 비교한 결과 기존의 방법과 새로운 방법 모두 플러터 풍속을 잘 예측하였다. 시간영역 공탄성 해석 결과는 두 단면에 대해 다른 결과를 보였는데, 실험방법 간의 차이는 매우 작았으나 하중제어 강제가진 실험 결과는 Causality condition을 상대적으로 크게 위반하며 두 가지

방법 모두 실제 교량의 움직임을 정확히 예측하지 못하였다. 이는 공기력이 교량의 움직임과 속도의 일차식으로 정의된다는 가정의 한계로 보이며, 교량의 움직임과 공기력의 비선형적 상호작용의 영향은 일반적인 교량에 대한 실험에서 무시할 만한 크기임을 보였다.

주요어: 플러터 계수; Equation error estimation; FDM-FIR 필터; 강제가진 실험; 공탄성 해석; 심플렉스 알고리즘

학번: 2013-20942